

The Role of Snow in Controlling Halogen Chemistry and Boundary Layer Oxidation During Arctic Spring: A 1D Modeling Case Study

Shaddy Ahmed, Jennie L. Thomas, Katie Tuite, Jochen Stutz, Frank Flocke, John J. Orlando, Rebecca S. Hornbrook, Eric C. Apel, Louisa K. Emmons, Detlev Helmig, et al.

▶ **To cite this version:**

Shaddy Ahmed, Jennie L. Thomas, Katie Tuite, Jochen Stutz, Frank Flocke, et al.. The Role of Snow in Controlling Halogen Chemistry and Boundary Layer Oxidation During Arctic Spring: A 1D Modeling Case Study. Journal of Geophysical Research: Atmospheres, 2022, 127, 10.1029/2021JD036140 . insu-03706386

HAL Id: insu-03706386

https://insu.hal.science/insu-03706386

Submitted on 28 Jun 2022

HAL is a multi-disciplinary open access archive for the deposit and dissemination of scientific research documents, whether they are published or not. The documents may come from teaching and research institutions in France or abroad, or from public or private research centers.

L'archive ouverte pluridisciplinaire **HAL**, est destinée au dépôt et à la diffusion de documents scientifiques de niveau recherche, publiés ou non, émanant des établissements d'enseignement et de recherche français ou étrangers, des laboratoires publics ou privés.



Distributed under a Creative Commons Attribution 4.0 International License

Check for updates

JGR Atmospheres

RESEARCH ARTICLE
10.1029/2021JD036140

The Role of Snow in Controlling Halogen Chemistry and Boundary Layer Oxidation During Arctic Spring: A 1D Modeling Case Study

Shaddy Ahmed[1], Jennie L. Thomas[1], Katie Tuite[2], Jochen Stutz[2], Frank Flocke[3], John J. Orlando[3], Rebecca S. Hornbrook[3], Eric C. Apel[3], Louisa K. Emmons[3], Detlev Helmig[4,5], Patrick Boylan[4], L. Gregory Huey[6], Samuel R. Hall[3], Kirk Ullmann[3], Christopher A. Cantrell[7,8], and Alan Fried[4,9]

[1]Université de Grenoble Alpes, CNRS, IRD, Grenoble INP, IGE, Grenoble, France, [2]Department of Atmospheric and Oceanic Sciences, University of California, Los Angeles, CA, USA, [3]Atmospheric Chemistry Observations & Modeling Laboratory, National Center for Atmospheric Research, Boulder, CO, USA, [4]Institute of Arctic and Alpine Research, University of Colorado, Boulder, CO, USA, [5]Boulder A.I.R. LLC, Boulder, CO, USA, [6]School of Earth and Atmospheric Sciences, Georgia Institute of Technology, Atlanta, GA, USA, [7]Department of Atmospheric and Oceanic Sciences (ATOC), University of Colorado, Boulder, CO, USA, [8]Laboratoire Interuniversitaire des Systèmes Atmosphériques (LISA), Creteil, France, [9]Earth Observing Laboratory, National Center for Atmospheric Research, Boulder, CO, USA

Key Points:

- A combination of factors including snow emissions, vertical mixing, and atmospheric chemistry explain surface Arctic halogen observations
- Snow emissions of halogens impact atmospheric chemistry within a shallow layer near the surface
- Surface HO_x concentrations are increased by up to a factor of 30 due to halogen chemistry

Supporting Information:

Supporting Information may be found in the online version of this article.

Correspondence to:

S. Ahmed and J. L. Thomas,
shaddy.ahmed@univ-grenoble-alpes.fr;
jennie.thomas@univ-grenoble-alpes.fr

Citation:

Ahmed, S., Thomas, J. L., Tuite, K., Stutz, J., Flocke, F., Orlando, J. J., et al. (2022). The role of snow in controlling halogen chemistry and boundary layer oxidation during Arctic spring: A 1D modeling case study. *Journal of Geophysical Research: Atmospheres*, *127*, e2021JD036140. https://doi.org/10.1029/2021JD036140

Received 9 NOV 2021
Accepted 22 FEB 2022

Author Contributions:

Conceptualization: Shaddy Ahmed, Jennie L. Thomas, Jochen Stutz
Data curation: Shaddy Ahmed, Frank Flocke, John J. Orlando, Rebecca S. Hornbrook, Eric C. Apel, Detlev Helmig, Patrick Boylan, L. Gregory Huey, Samuel R. Hall, Kirk Ullmann, Christopher A. Cantrell, Alan Fried
Formal analysis: Shaddy Ahmed, Jennie L. Thomas, Katie Tuite, Jochen Stutz
Funding acquisition: Jennie L. Thomas
Investigation: Shaddy Ahmed
Methodology: Shaddy Ahmed, Jennie L. Thomas, Katie Tuite, Jochen Stutz

© 2022. The Authors.
This is an open access article under the terms of the Creative Commons Attribution License, which permits use, distribution and reproduction in any medium, provided the original work is properly cited.

Abstract Reactive chlorine and bromine species emitted from snow and aerosols can significantly alter the oxidative capacity of the polar boundary layer. However, halogen production mechanisms from snow remain highly uncertain, making it difficult for most models to include descriptions of halogen snow emissions and to understand the impact on atmospheric chemistry. We investigate the influence of Arctic halogen emissions from snow on boundary layer oxidation processes using a one-dimensional atmospheric chemistry and transport model (PACT-1D). To understand the combined impact of snow emissions and boundary layer dynamics on atmospheric chemistry, we model Cl_2 and Br_2 primary emissions from snow and include heterogeneous recycling of halogens on both snow and aerosols. We focus on a 2-day case study from the 2009 Ocean-Atmosphere-Sea Ice-Snowpack campaign at Utqiaġvik, Alaska. The model reproduces both the diurnal cycle and high quantity of Cl_2 observed, along with the measured concentrations of Br_2, BrO, and HOBr. Due to the combined effects of emissions, recycling, vertical mixing, and atmospheric chemistry, reactive chlorine is typically confined to the lowest 15 m of the atmosphere, while bromine can impact chemistry up to and above the surface inversion height. Upon including halogen emissions and recycling, the concentration of HO_x ($HO_x = OH + HO_2$) at the surface increases by as much as a factor of 30 at mid-day. The change in HO_x due to halogen chemistry, as well as chlorine atoms derived from snow emissions, significantly reduce volatile organic compound lifetimes within a shallow layer near the surface.

1. Introduction

Halogen chemistry has a large impact on tropospheric chemistry in the polar regions (e.g., Abbatt et al., 2012; Barrie et al., 1988; Oltmans et al., 2012; Simpson et al., 2007, 2015; Steffen et al., 2008, 2013). Recently, new evidence of active Arctic chlorine chemistry has been attributed mainly to photochemical activation of chloride present in surface snow (Custard et al., 2017; Liao et al., 2014). Molecular chlorine (Cl_2) and nitryl chloride ($ClNO_2$), emitted from snow and aerosols, are sources of atomic chlorine (Cl) following their photolysis (McNamara et al., 2019, 2021). The highly reactive nature of Cl atoms makes it important even in trace amounts as Cl atoms react with volatile organic compounds (VOCs) up to three orders of magnitude faster than the more abundant hydroxyl radical (OH) (Atkinson et al., 2006). Active chlorine chemistry occurs simultaneously with reactive bromine chemistry each spring (e.g., Abbatt et al., 2012; Barrie et al., 1988; Simpson et al., 2007, 2015). The latter causes both ozone (O_3) and mercury depletion (Hg^0) in the lowest part of the atmosphere (e.g., Oltmans et al., 2012; Steffen et al., 2008, 2013).

Halogens in the Arctic atmosphere ultimately originate from the ocean as halides (Cl^- and Br^-), which are activated on salty surfaces such as snow on sea ice, continental snow and aerosols (Abbatt et al., 2012). Chlorine and bromine species impact atmospheric chemistry within the polar boundary layer via reactions (R1–R9; where X, Y = Cl or Br) (Abbatt et al., 2012; Simpson et al., 2015). Cl_2 photolyzes very quickly during the day (R1), with

Project Administration: Jennie L. Thomas
Resources: Jennie L. Thomas, Eric C. Apel
Software: Shaddy Ahmed, Jennie L. Thomas, Katie Tuite, Jochen Stutz
Supervision: Jennie L. Thomas, Jochen Stutz
Validation: Jennie L. Thomas, Jochen Stutz, Frank Flocke, John J. Orlando, Rebecca S. Hornbrook, Detlev Helmig, Patrick Boylan, L. Gregory Huey, Samuel R. Hall, Kirk Ullmann, Christopher A. Cantrell, Alan Fried
Visualization: Shaddy Ahmed
Writing – original draft: Shaddy Ahmed, Jennie L. Thomas
Writing – review & editing: Shaddy Ahmed, Jennie L. Thomas, Katie Tuite, Jochen Stutz, Frank Flocke, John J. Orlando, Rebecca S. Hornbrook, Eric C. Apel, Detlev Helmig, Patrick Boylan, L. Gregory Huey, Samuel R. Hall, Kirk Ullmann, Christopher A. Cantrell, Alan Fried

a photolysis lifetime of approximately 10 min, producing Cl atoms that rapidly react with ozone (R2) or VOCs (including methane) ([R3] and [R4]) (Atkinson et al., 2006). Reactions (R3) and (R4) constitute the major reaction pathways of Cl atoms (Platt & Hönninger, 2003). This produces organic peroxy radicals (RO_2), including the methylperoxy radical (CH_3O_2), which ultimately contribute to hydroperoxyl radical formation (HO_2). HO_2 production, driven by chlorine chemistry, can impact HO_x chemistry (HO_x = OH + HO_2) by decreasing the OH/HO_2 ratio, as well as affecting the reactive bromine cycle (Piot & von Glasow, 2009; Rudolph et al., 1999; Thompson et al., 2015). Molecular bromine (Br_2) is photolyzed very rapidly (photolysis lifetime <1 min) to produce bromine atoms (Br) which can lead to efficient ozone destruction and formation of bromine monoxide (BrO) (Wang et al., 2019). However, Br atoms react appreciably only with a few specific VOCs such as ethyne and the aldehydes and not with methane ([R3] and [R4] only occur for Cl). Br atoms can also react with elemental mercury to deplete near-surface atmospheric Hg^0 levels and produce more reactive forms of mercury (Hg^{II}) (Steffen et al., 2008, 2013; Wang et al., 2019). Subsequent reaction of BrO with HO_2 forms HOBr (R5), which can be photolyzed to re-form Br and OH (R6). The net result of reactions (R5) and (R6) is the regeneration of a Br atom, which can facilitate further ozone depletion, and the conversion of HO_2 to OH, increasing the oxidative capacity of the atmosphere. At high BrO concentrations, Br_2 is also regenerated in the gas phase via self-reaction of BrO (R7).

$$X_2 \xrightarrow{h\nu} 2X \quad \text{(R1)}$$

$$X + O_3 \rightarrow XO + O_2 \quad \text{(R2)}$$

$$Cl + RH + O_2 \rightarrow RO_2 + HCl \quad \text{(R3)}$$

$$Cl + CH_4 \rightarrow CH_3 + HCl \quad \text{(R4)}$$

$$XO + HO_2 \rightarrow HOX + O_2 \quad \text{(R5)}$$

$$HOX \xrightarrow{h\nu} X + OH \quad \text{(R6)}$$

$$BrO + BrO \rightarrow Br_2 + O_2 \quad \text{(R7)}$$

Figure 1a highlights the typical diurnal behavior of surface molecular halogen concentrations, snow emissions, solar radiation, and the boundary layer height observed during Arctic spring. Measured diurnal cycles of Cl_2 have shown a double-peaked profile, with peaks in the morning and late afternoon, followed by concentrations dropping below 0.8 parts per trillion by volume (pptv) after midnight (Custard et al., 2016; Liao et al., 2014; McNamara et al., 2019). At sunrise, increased solar radiation drives photochemistry within the snow interstitial air which leads to the release of halogens to the overlying atmosphere via diffusion and wind pumping (Bartels-Rausch et al., 2014; Grannas et al., 2007; Pratt et al., 2013; Thomas et al., 2011; Toyota et al., 2014). Boundary layer mixing modulates surface Cl_2 concentrations, with Cl_2 decreasing during the day due to a combination of its fast photolytic loss (R1) and the effects of boundary layer mixing. Solar heating of the lower atmosphere can cause turbulent mixing of the surface layer, mixing species away from the surface, and increasing the height of the boundary layer (Anderson & Neff, 2008). Low light conditions (i.e., night and early morning) cause a reduction in the photochemical loss of Cl_2 (R1) and a collapse of the boundary layer. This effect has previously been demonstrated to drive evening increases of reactive nitrogen species (NO_x = NO + NO_2) at the surface in both the Arctic and Antarctic (Frey et al., 2015; Honrath et al., 1999, 2002; Thomas et al., 2011).

Figure 1b illustrates some of the key known emission sources of halogens from surface snow in the Arctic. Heterogeneous reactions involving hypohalous acids (e.g., HOCl and HOBr; R8) and halogen nitrates (e.g., $ClONO_2$ and $BrONO_2$; R9), have been recognized as a source of molecular halogens on halide-containing snow and aerosol surfaces (Aguzzi & Rossi, 1999; Deiber et al., 2004; Finlayson-Pitts et al., 1989; Hu et al., 1995; Pratte & Rossi, 2006). Bromine chloride (BrCl) is another product formed via reactions (R8) and (R9) on snow and aerosols, linking the chlorine and bromine chemical cycles (McNamara et al., 2020). BrCl can then be photolyzed, re-forming Br and Cl atoms, as in reaction (R1).

$$HOX + X^-/Y^- + H^+ \xrightarrow{(surface)} X_2/XY + H_2O \quad \text{(R8)}$$

$$XONO_2 + X^-/Y^- \xrightarrow{(surface)} X_2/XY + NO_3^- \quad \text{(R9)}$$

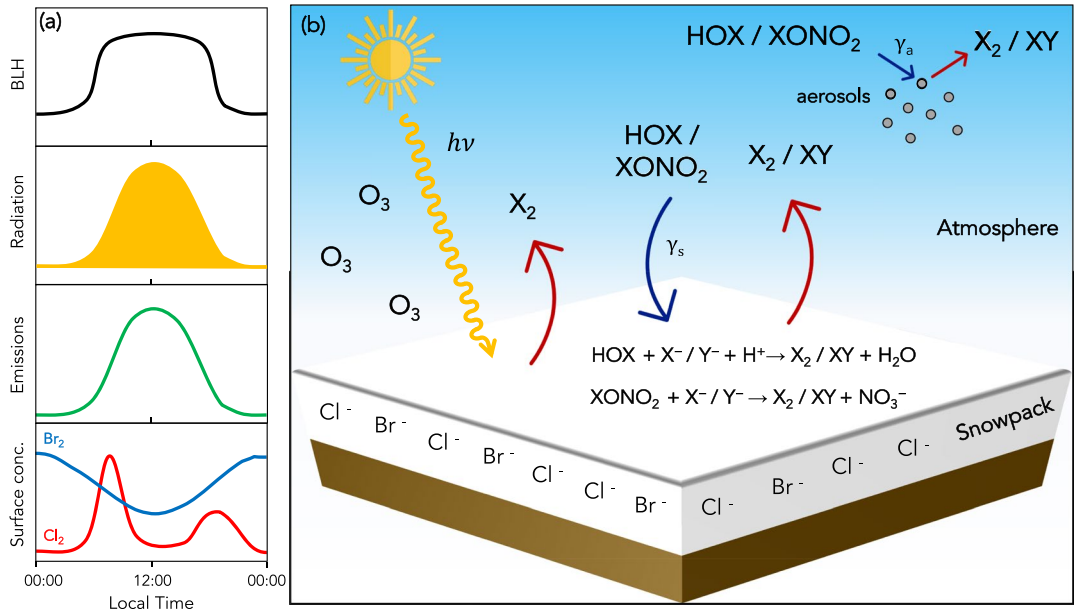


Figure 1. (a) Diurnal evolution of boundary layer height (BLH), solar radiation, chemical snowpack emissions, and surface concentrations of Cl_2 and Br_2 for an "average" day in the Arctic during spring (not drawn to scale). (b) Schematic of key polar halogen emissions from the continental snowpack (X = Cl, Br). Blue arrows represent loss processes and red arrows indicate production. Primary production of halogens is based on ozone and the availability of sunlight. Molecular halogens are also emitted via surface snow and aerosol recycling reactions, dependent on the heterogeneous reactive uptake coefficients γ_s and γ_a, on surface snow and aerosols, respectively.

At present, detailed descriptions of chlorine snow emissions remain absent from most 3D numerical models. Bromine mechanisms are included in some 3D models, but remain under discussion as to the source and recycling mechanisms involving snow (Falk & Sinnhuber, 2018; Fernandez et al., 2019; Herrmann et al., 2021; Marelle et al., 2021; Toyota et al., 2011). Snow is a very complex photochemical medium and the release of halogens is determined by many uncertain processes/variables, including: snow physics; snow/ice chemistry (including photochemistry); gas transport within snow; and impurity concentrations and locations (Bartels-Rausch et al., 2014; Domine et al., 2008; Grannas et al., 2007; McNeill et al., 2012). As a result, modeling snow-covered environments using a first principles approach remains challenging and uncertain (Domine et al., 2013). Zero-dimensional box models are often used to study the effects of halogens on boundary layer chemistry under Arctic conditions (Custard et al., 2015; Liao, Huey, Tanner, et al., 2012; Liao et al., 2014; McNamara et al., 2020; Piot & von Glasow, 2009; Thompson et al., 2015; Wang & Pratt, 2017). An inherent limitation of 0D models, however, is the absence of the vertical dimension necessary for simulating vertical transport and capturing concentration gradients in the atmosphere. Additionally, the physical conditions that characterize the polar regions (low temperatures, limited sunlight during winter, high albedo, etc.) can often create stable low-level temperature inversions resulting in shallow boundary layers (Kahl, 1990). This can greatly impact the vertical distribution of chemical species by acting as a barrier to vertical mixing and transport. One-dimensional models are therefore extremely useful tools which can include these processes to help us better understand the interactions between snow and the atmosphere (Cao et al., 2016; Herrmann et al., 2019; Lehrer et al., 2004; Piot & von Glasow, 2008; Thomas et al., 2012, 2011; Toyota et al., 2014; Wang et al., 2020).

The first observations of high Cl_2 levels within the Arctic boundary layer were reported in spring 2009, during the Ocean-Atmosphere-Sea Ice-Snowpack (OASIS) campaign at Utqiaġvik, Alaska (Liao et al., 2014). Cl_2 mixing ratios of up to 400 pptv were observed and an average noontime Cl atom concentration of 2×10^5 atoms cm^{-3} was estimated from these observations. Daytime Cl_2 mixing ratios were highly correlated with sunlight and surface ozone levels (r^2 value = 0.86), indicating both are key requirements for Cl_2 production. Measurements of VOCs made during the campaign showed a clear impact of chlorine chemistry on VOC oxidation processes (Hornbrook et al., 2016). Measurement-derived estimates of Cl atom concentration suggested the presence of a highly reactive surface layer, which led to an overprediction of VOC production and loss rates compared to the observations

Table 1
Measurements From the OASIS 2009 Campaign Used in This Study

Measurement	Method	Reference
Meteorology and turbulent fluxes	Ultrasonic anemometers	Boylan et al. (2014)
Cl_2, Br_2, BrO, HOBr	Chemical Ionization Mass Spectrometers (CIMS)	Liao et al. (2011, 2014); Liao, Huey, Tanner, et al. (2012)
OH, HO_2	Chemical Ionization Mass Spectrometers (CIMS)	Hornbrook et al. (2011); Mauldin III et al. (1998); Tanner et al. (1997)
NO, NO_2, O_3	Chemiluminescence	Helmig et al. (2012); Villena et al. (2011); Weinheimer et al. (1998)
HCHO	Difference Frequency Generation Tunable Diode Laser Absorption Spectrometer	Weibring et al. (2007, 2010)
CO	IR absorption CO analyzer	Parrish et al. (1994)
VOCs[a]	Trace Organic Gas Analyzer (TOGA)	Hornbrook et al. (2016)
Aerosol number density and radius	Optical Particle Counter (OPC) and Scanning Mobility Particle Sizers (SMPS)	Woo et al. (2001)
Actinic flux	CCD Actinic Flux Spectroradiometers (CAFS)	Shetter and Müller (1999)

[a]See Table 1 in Hornbrook et al. (2016).

(Hornbrook et al., 2016). Interactions between radical chemistry, atmospheric mixing, and snow emissions need to be better understood in order to fully explain these observations and the impacts of halogens on boundary layer oxidation processes.

In this work, we address the following questions:

1. What combination of factors, including vertical mixing, land-based snow emissions/recycling, and chemistry explain observations of halogens in the Arctic surface layer?
2. How are halogens vertically distributed within the polar boundary layer?
3. What is the impact of halogen chemistry on boundary layer oxidation processes as a function of altitude?

We answer these questions using an updated version of the Platform for Atmospheric Chemistry and vertical Transport in 1-dimension (PACT-1D) model (Tuite et al., 2021), which includes descriptions of halogen chemistry, emissions, and recycling. We compare our model with surface measurements of chemical species, including Cl_2 and Br_2, recorded during the 2009 OASIS campaign at Utqiaġvik, Alaska. In Section 2, we introduce the measurements used from the campaign and the new model halogen updates are described in Section 3. The model configuration used in this work is presented in Section 4, followed by the model results and a discussion in Section 5. Finally, the conclusions and perspectives are presented in Section 6.

2. OASIS 2009 Campaign Measurements

In this study, we use measurements taken during the OASIS campaign, which was conducted between March and April 2009 near Utqiaġvik, Alaska. The measurement site was located approximately 5.5 km northeast of the town of Utqiaġvik (71.323 N, 156.663 W; 8 m above sea level) and was chosen for the prevailing northeasterly winds arriving from over the Beaufort Sea. A map of the study site can be found in Boylan et al. (2014) and Hornbrook et al. (2016). Observations from this campaign were chosen due to the extensive chemical and meteorological measurements available, including direct measurements of Cl_2, Br_2, BrO, and a large number of VOCs. A summary of the measurements used in this study is given in Table 1 with the respective instruments/techniques used during OASIS. Meteorological measurements (temperature, winds, relative humidity) were made from two tower stations set up at the field site at several heights. At one of the tower stations, turbulent flux measurements were made using ultrasonic anemometers located at 4 heights (0.6, 1.8, 3.2, and 6.2 m above ground level [AGL]). Inorganic halogens (including Cl_2, Br_2, BrO and HOBr), as well as OH and HO_2, were measured using chemical ionization mass spectrometers (CIMS) at 1.5 m AGL (Hornbrook et al., 2011; Liao et al., 2011, 2014; Liao, Huey, Tanner, et al., 2012; Mauldin III et al., 1998; Tanner et al., 1997). Surface ozone and NO_x measurements were made using

Table 2
Heterogeneous Reactions and Reaction Uptake Coefficients on Aerosols (γ_a)

Reaction	Heterogeneous reactive uptake (γ_a)	Reference
$HOCl + Cl^-_{(aq)} \rightarrow Cl_2$	2×10^{-4}	Ammann et al. (2013)
$HOCl + Br^-_{(aq)} \rightarrow BrCl$	2×10^{-4}	Ammann et al. (2013)
$ClONO_2 + Cl^-_{(aq)} \rightarrow Cl_2 + HNO_{3(aq)}$	0.03	Aguzzi and Rossi (1999)
$ClONO_2 + Br^-_{(aq)} \rightarrow BrCl + HNO_{3(aq)}$	0.05	Aguzzi and Rossi (1999)
$ClONO_2 \rightarrow HOCl + HNO_{3(aq)}$	0.03	Aguzzi and Rossi (1999)
$HOBr + Br^-_{(aq)} \rightarrow Br_2$	0.05	Pratte and Rossi (2006); IUPAC (2009)
$HOBr + Cl^-_{(aq)} \rightarrow BrCl$	0.05	Pratte and Rossi (2006); IUPAC (2009)
$BrONO_2 + Br^-_{(aq)} \rightarrow Br_2$	0.06	Deiber et al. (2004)
$BrONO_2 + Cl^-_{(aq)} \rightarrow BrCl$	0.04	Deiber et al. (2004)
$BrONO_2 \rightarrow HOBr + HNO_{3(aq)}$	0.04	Deiber et al. (2004)
$N_2O_5 + Cl^-_{(aq)} \rightarrow ClNO_2 + HNO_{3(aq)}$	0.02	Burkholder et al. (2019)
$N_2O_5 + Br^-_{(aq)} \rightarrow BrNO_2 + HNO_{3(aq)}$	0.011	Seisel et al. (1998)
$Cl_2 + Br^-_{(aq)} \rightarrow BrCl + Cl^-_{(aq)}$	0.2	Burkholder et al. (2019)
$OH + HCl \rightarrow 0.5 * Cl_2$	0.1	Knipping et al. (2000); Laskin et al. (2006)

a chemiluminescence instrument on a second tower station, operated by the National Center for Atmospheric Research (NCAR), at 3 different heights (0.6, 1.5, and 5.4 m AGL) (Helmig et al., 2012; Villena et al., 2011; Weinheimer et al., 1998). Additionally, measurements of formaldehyde (HCHO) made by a Difference Frequency Generation Tunable Diode Laser Absorption Spectrometer (Barret et al., 2011; Weibring et al., 2007, 2010), and 18 VOCs measured by a Trace Organic Gas Analyzer (TOGA) (Hornbrook et al., 2016) were made at these same heights. Balloon soundings were also launched during the campaign to record vertical profiles of ozone (Helmig et al., 2012; Oltmans et al., 2012). Carbon monoxide (CO) measurements were made using a CO infrared absorption analyzer (Parrish et al., 1994). Aerosol physical properties (size distribution and number concentration) were measured using an optical particle counter and two scanning mobility particle sizers (Woo et al., 2001). Finally, actinic flux measurements made by CCD Actinic Flux Spectroradiometers (CAFS) were used to calculate photolysis frequencies of 35 different reactions using a modified version of the Tropospheric Ultraviolet and Visible (TUV) radiation model version 4.4 (Madronich & Flocke, 1999; Shetter & Müller, 1999). Data from this campaign are available through the National Science Foundation (NSF) Arctic Data Center at https://arcticdata.io/ (Apel, 2009; Cantrell, 2009; Fried, 2009; Guenther, 2009; Hall, 2009; Smith et al., 2009; Weinheimer, 2009).

3. Description of Halogen Chemistry Within PACT-1D

The Platform for Atmospheric Chemistry and vertical Transport in 1-Dimension (PACT-1D) is the vertical column model used in this work to study Arctic halogen emissions and their impact on oxidation processes during the OASIS campaign. A full description of this model is given in Tuite et al. (2021). Chlorine and bromine gas-phase and heterogeneous reactions are added to this version of the model. Snow emissions and recycling mechanisms of chlorine and bromine have also been implemented and are described in the following sections.

3.1. Gas-Phase and Aerosol Heterogeneous Halogen Chemistry

We update the existing PACT-1D mechanism to include additional chlorine and bromine gas-phase and heterogeneous reactions. The chemical mechanism in PACT-1D is based on the Regional Atmospheric Chemistry Mechanism version 2 (RACM2) (Goliff et al., 2013) using the Kinetic PreProcessor (KPP) (Sandu & Sander, 2006). The additional gas-phase bromine reactions are added following the implementation of Marelle et al. (2021) and are listed in the model chemical mechanism (Ahmed et al., 2022). Reactive and non-reactive heterogeneous uptake reactions of halogens on aerosols are also added to the model (Table 2). We do not include a full description of aerosol aqueous-phase chemistry within the model. We track particulate chloride and bromide as separate species that undergo heterogeneous chemistry to ensure mass balance, which are tracked in the model. We do this by first

initializing the concentration of aerosol-phase chloride and bromide to the chloride and bromide concentrations in fresh sea salt aerosols and then track release and reactive and non reactive uptake. Second-order heterogeneous reactions consuming aerosol-phase halide ions are treated as pseudo first-order reactions, following Marelle et al. (2021), maintaining mass conservation of each species.

3.2. Snow Emission and Recycling of Cl_2 and Br_2

Emissions of molecular halogens from snow have been identified as a key source of Arctic halogen production (Custard et al., 2017; Pratt et al., 2013). Cl_2 and Br_2 production from continental snow have been reported to be a function of both solar radiation and ozone concentration (Custard et al., 2017; Liao et al., 2014; Liu et al., 2017). Halogen species deposited to the snow surface can also undergo recycling mechanisms to re-emit reactive halogens back into the atmosphere (Abbatt et al., 2012; Toyota et al., 2011). We therefore add four parameterizations to describe emissions of Cl_2 and Br_2 in this version of PACT-1D. We include (a) an emission of Cl_2 and Br_2 as a function of the available solar radiation and the surface ozone concentration, and (b) a recycling source of X_2 from the surface conversion of $XONO_2$ and HOX (where X = Cl, Br) on snow. In both cases, the exact parameterizations are determined by comparing modeled and observed halogen concentrations.

The emission of Cl_2 is parameterized as follows:

$$E_{Cl_2}^{primary} = F_{(p,Cl)} \times \left(J_{Cl_2}\right)^{0.5} \times [O_3] \quad (1)$$

$$E_{Cl_2}^{recycling} = \gamma_{(snow,Cl)} \times \left(D_{ClONO_2} + D_{HOCl}\right) \quad (2)$$

where $E_{Cl_2}^{primary}$ and $E_{Cl_2}^{recycling}$ are the snow emission fluxes of Cl_2, $F_{(p,Cl)}$ is a correction factor which includes a scaling term and the height of the lowest model level (0.01 cm) in units of cm $s^{-\frac{1}{2}}$, J_{Cl_2} is the calculated photolysis rate of Cl_2, $[O_3]$ is the measured O_3 concentration (in molec cm^{-3}), $\gamma_{(snow,Cl)}$ is the probability of heterogeneous conversion on snow to re-form Cl_2 (between 0 and 1), and D_{ClONO_2} and D_{HOCl} are the model-calculated deposition rates of $ClONO_2$ and HOCl, respectively. In the case of primary Cl_2 emissions (Equation 1), different values of $F_{(p,Cl)}$ were tested in order to reproduce the Cl_2 measurement data in the model (Figure S1 in Supporting Information S1). Observed ambient concentrations of Cl_2 showed a double peaked profile, with an increase in the early morning following sunrise, and a second peak in the late afternoon before falling to almost zero at night. The best-fit primary emission flux for Cl_2 is found to be a function of J_{Cl_2} to the power of 0.5, with $F_{(p,Cl)} = 0.2$ cm $s^{-\frac{1}{2}}$. It is also well known that $ClONO_2$ and HOCl are converted on ice surfaces to re-form Cl_2 (IUPAC, 2009). However, within snow there are a number of complex physical and chemical processes that make these recommendations not directly applicable for snow. We therefore performed a series of sensitivity tests varying $\gamma_{(snow,Cl)}$ between 0 and 1, and found the best fit value of 0.1 for chlorine recycling on snow (Figure S2 in Supporting Information S1).

For Br_2, the emission sources are described as:

$$E_{Br_2}^{primary} = F_{(p,Br)} \times J_{Br_2} \times [O_3] \quad (3)$$

$$E_{Br_2}^{recycling} = \gamma_{(snow,Br)} \times \left(D_{BrONO_2} + D_{HOBr}\right) \quad (4)$$

where $E_{Br_2}^{primary}$ and $E_{Br_2}^{recycling}$ are the snow emission fluxes of Br_2, $F_{(p,Br)}$ is a correction factor which includes a scaling term and the height of the lowest model level (0.01 cm) in units of cm, J_{Br_2} is the calculated photolysis rate of Br_2, $\gamma_{(snow,Br)}$ is the heterogeneous conversion efficiency on snow to re-form Br_2 (between 0 and 1), and D_{BrONO_2} and D_{HOBr} are the model-calculated deposition rates of $BrONO_2$ and HOBr, respectively. For bromine, we found that the observations of bromine species are best described using primary emissions (Equation 3) as a function of J_{Br_2}, with $F_{(p,Br)} = 0.01$ cm (equivalent to the lowest model level height and a scaling factor of 1). The conversion of $BrONO_2$ and HOBr on ice to re-form Br_2 is known to be more efficient than for chlorine (IUPAC, 2009), which in part facilitates the well known bromine explosion chemistry (Abbatt et al., 2012). We tested a range of possible conversion efficiencies for these reactions and found $\gamma_{(snow,Br)} = 0.6$ best reproduces the observations (Figure S3 in Supporting Information S1). For both Equations 2 and 4, it is assumed that there is an infinite supply of Cl^- and Br^- in the snow. We do not include conversion of N_2O_5 on snow to form reactive bromine and chlorine due to the low NO_x concentrations compared to pollution influence.

There are large uncertainties in describing both the primary emission flux (Equations 1 and 3) from land-based snow, as well as the recycling of both bromine and chlorine species on snow (Equations 2 and 4), which must be considered in future work that use or further refine these parameterizations. First, there are significant uncertainties in vertical transport near the snow surface and in the lowest portion of the atmosphere (~below 10 m). Therefore, as future work refines our knowledge of these vertical transport processes, we will need to revisit the values used for $F_{(p,\mathrm{Cl})}$, $F_{(p,\mathrm{Br})}$, $\gamma_{(snow,\mathrm{Cl})}$ and $\gamma_{(snow,\mathrm{Br})}$. Second, the main factors driving molecular halogen production from the snowpack are still highly uncertain, with more work needed to improve our understanding. In addition, descriptions of halogen emissions from land-based snow within 3D models remain limited. Bromine emissions triggered from ozone deposition to snow on sea ice is the main process considered by the bromine emissions/recycling scheme of Toyota et al. (2011). Here, we use ambient ozone concentrations rather than ozone deposition as the trigger for both bromine and chlorine on land-based snow, as suggested from observations. Our equations can be re-formulated as a function of the ozone deposition rate (which is directly dependant on ozone concentration) to be more consistent with equations proposed for snow on sea ice. Finally, production of BrCl from Arctic snow has been measured following irradiation of the snowpack, with multiphase reactions on snow also predicted to be significant contributors of BrCl production (Custard et al., 2017; McNamara et al., 2020). However, flux estimates of BrCl from snow remain uncertain and measurements of BrCl were not available during our selected simulation period (see Section 4.1). We therefore only include BrCl production via heterogeneous reactions on aerosols (Table 2), but, this must be updated in future work to also include BrCl emissions from continental snow.

4. Model Setup

4.1. Selection of OASIS Simulation Period

The model was set up for the dates of 18–19 March 2009 during the campaign; these dates were selected due to the high Cl_2 concentrations recorded and the limited influence from local pollution sources (Figure S4 in Supporting Information S1). The average daytime (06:00–20:00) Cl_2 mixing ratio for the 2 days was 59 pptv and surface ozone levels remained above 10 parts per billion by volume (ppbv), indicating that there was not a major ozone depletion event during this period. Ozonesonde data from profiles launched at the start and just after our modeling case study showed that ozone was well distributed within the lower atmosphere with no significant ozone gradients as a function of altitude (Figure 4c in Oltmans et al. (2012) and Figure 13a in Helmig et al. (2012)). Average background levels of NO_x and CO over the entire campaign were recorded at ~84 pptv and ~160 ppbv, respectively (Villena et al., 2011). Measurements of NO_x and CO between 18 and 19 March do not suggest polluted conditions, with CO levels close to the average background measurements (~160 ppbv), however NO_x levels were above the average background levels (50–500 pptv). Influence from nearby anthropogenic sources was likely to be minimal during this period as winds arriving at the measurement site originated from the Arctic Ocean (north through northeast) for most of 18 and 19 March. Considering these criteria, the period between 18 and 19 March best met the requirements for our modeling case study.

Figures 2a and 2b show the state of sea ice north of Utqiaġvik, on the 18 and 19 March, respectively. A key feature of Figures 2a and 2b is the presence of sea ice leads close to the measurement site. Sea ice leads are visible on both days which are important as they can induce convective mixing of air masses, impacting the concentration of species recorded at the measurement site (Moore et al., 2014). This has been shown to replenish ozone-depleted air masses to near-background concentrations (Moore et al., 2014) as well as influencing the vertical distribution of BrO by mixing it higher in the atmosphere (Simpson et al., 2017).

4.2. Model Configuration

We set up the vertical model grid (Figure 3a) using a total of 112 levels, with a logarithmic spacing for the lowest 1 m of the grid down to a lower boundary of 1×10^{-4} m. The model levels are linearly spaced up to 100 m, by 1-m increments, followed by a non-linear spacing to an upper boundary of 3,000 m. This highly resolved vertical model grid allows us to analyze the impacts of halogen emissions on chemistry very close to the surface.

The 1D model is driven by input data obtained from the measurements (where possible), model output data and calculated explicitly from parameterizations. The atmospheric dynamics (temperature, pressure, relative humidity) are calculated using the 3D Weather Research and Forecasting (WRF) meteorological model (Skamarock et al., 2019) for Utqiaġvik, Alaska, and used to drive the 1D model physics in combination with the OASIS ground

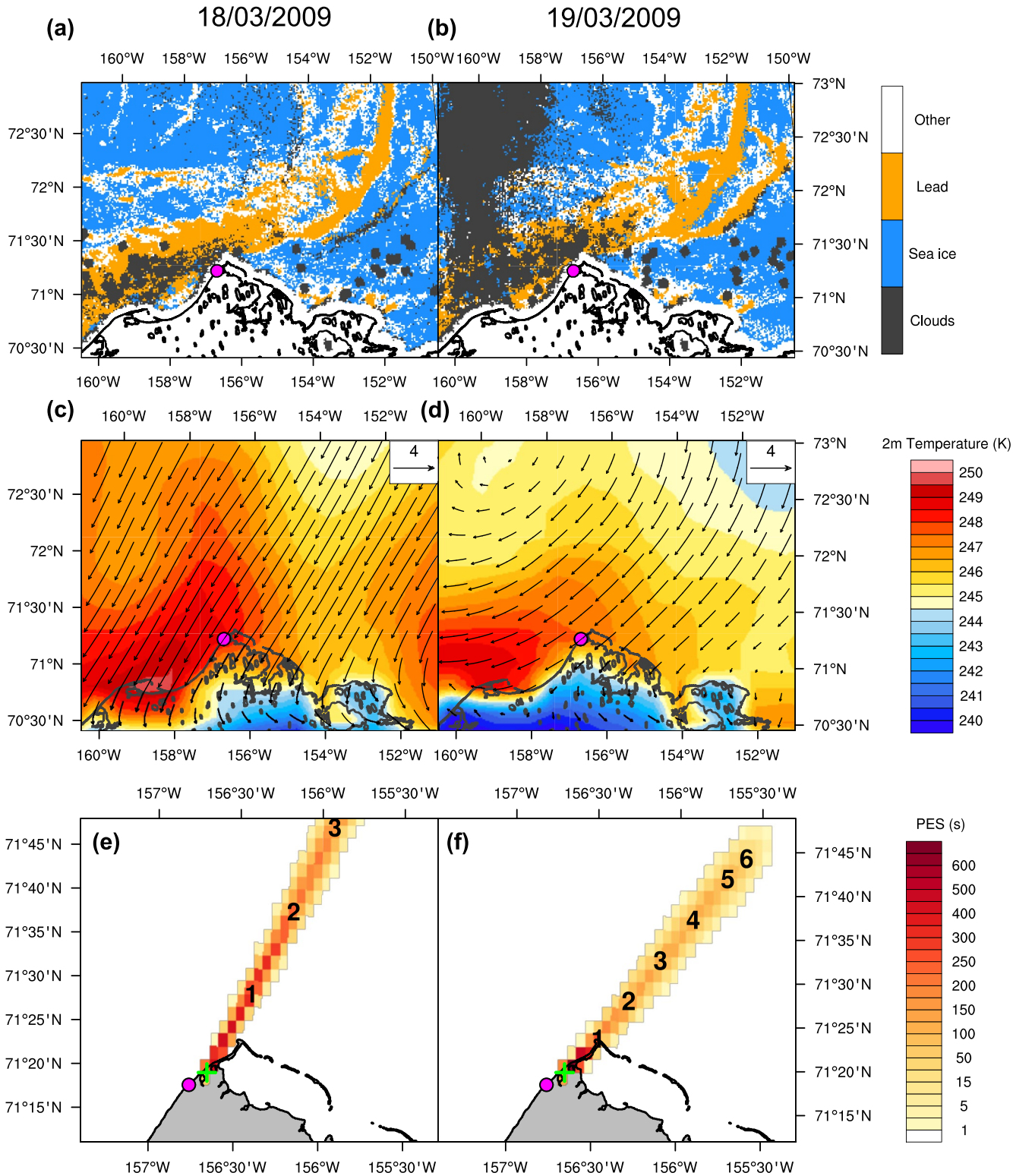


Figure 2. (a) Daily Arctic sea ice cover and leads from Willmes and Heinemann (2015) over Northern Alaska on 18 March 2009 and (b) 19 March 2009 with the town of Utqiaġvik marked in magenta. Areas shaded in white represent either land cover or data artifacts. (c) 2-m temperature from WRF over Utqiaġivk at local noon on 18 March 2009 and (d) 19 March 2009 with 10-m wind speed and wind directions displayed as arrows. (e) FLEXPART-WRF 6-hr backwards surface (0–100 m) potential emission sensitivity (PES) from the measurement site (marked by the green cross) on 18 March 2009–10:00 AKST and (f) 19 March 2009–18:00 AKST. Numbers represent hourly intervals since release.

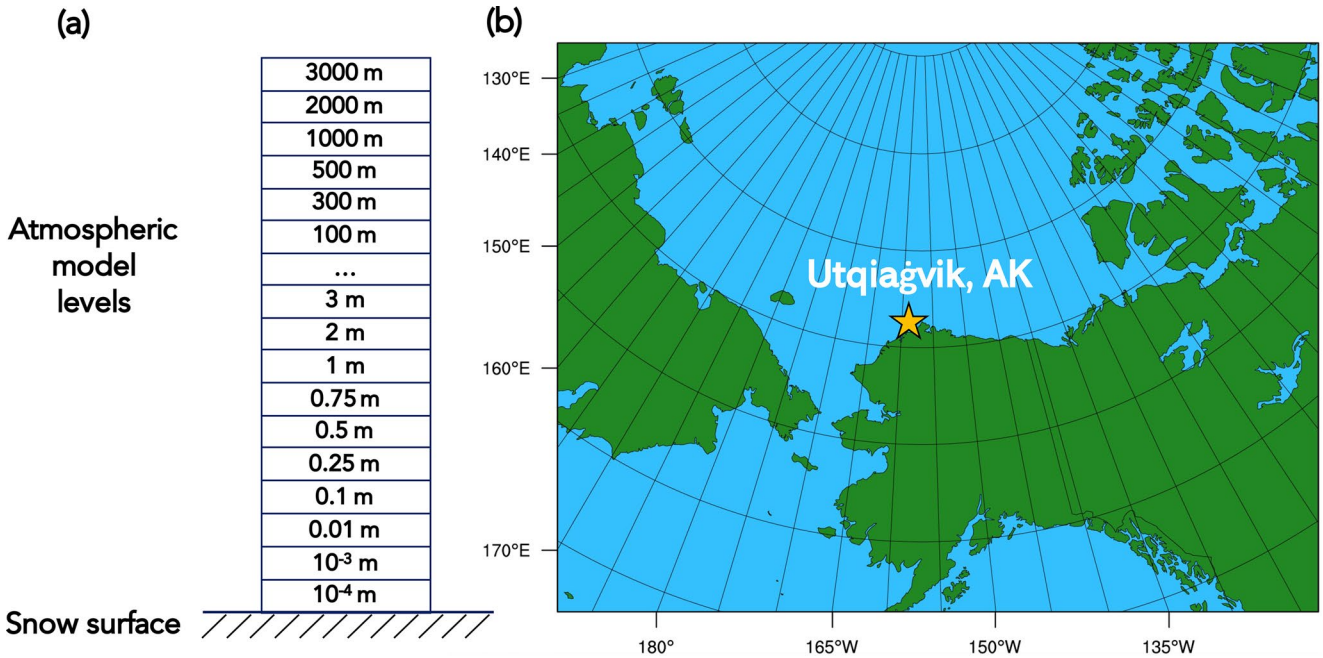


Figure 3. (a) PACT-1D model grid used with numbers representing the upper model level height in meters above the snow surface. A total of 112 vertical model levels were used. (b) 3D WRF model domain centered on Utqiaġvik, Alaska with a 25 × 25 km horizontal resolution and 50 vertical levels up to a pressure of 50 hPa.

measurements. We use a WRF set up specifically optimized for the Arctic, described in Marelle et al. (2017), with the model domain centered at Utqiaġvik (domain shown in Figure 3b). A horizontal resolution of 25 km × 25 km is used with a vertical resolution of 50 levels, up to a pressure of 50 hPa. To validate the use of the WRF simulated meteorology, we compare WRF calculated temperatures at Utqiaġvik with surface measurements from OASIS and available vertical temperature profiles in Figure 4. The Integrated Global Radiosonde Archive (IGRA, Durre et al. (2006)) provides radiosonde data twice a day at 00:00 and 12:00 UTC (15:00 and 03:00 AKST, UTC-9, respectively) which we use to compare with our model results. Figure 4 shows that we are able to obtain very good agreement of both the surface and vertical temperature profiles in WRF compared to the observations.

The eddy diffusion coefficients (K_z) in the model are calculated following the parameterization described in Cao et al. (2016) and used in Herrmann et al. (2019). We calculate these values as measurement data of eddy diffusion coefficients during this period were sparse. Vertical K_z profiles are calculated using the measured friction velocities (u_*) at 1.8 m AGL, with the estimated surface inversion height (SIH) derived from the tower turbulent flux measurements. A comparison was made between the calculated K_z values and the available measurement data which showed that calculated values were approximately a factor of 3 greater than the observations. Above the surface inversion layer, we assume a fixed value of $K_z = 1\ \mathrm{cm^2\ s^{-1}}$, following Cao et al. (2016). In our model runs, we calculate the SIH using a description based on eddy viscosity scaling, following Equation 5 (Zilitinkevich & Baklanov, 2002; Zilitinkevich et al., 2002):

$$\mathrm{SIH} = C_s^2 (u_* L / |f|)^{0.5} \tag{5}$$

where C_s is an empirical constant (estimated as 0.7), u_* is the measured friction velocity, L is the calculated Obukhov length from the measurements and f is the Coriolis parameter (equal to 1.38×10^4 at the latitude of the study site).

Chemical concentrations in the model are initialized using both observations and CAM-chem model data (Buchholz et al., 2019; Emmons et al., 2020). Aerosol surface area and number concentration are fixed to the observations for the duration of the run throughout the boundary layer. To supplement the 35 reactions reported in the CAFS data set, additional photolysis rates were added using the TUV radiation model (version 5.0). Each of these additional rates is scaled to the reported NO_2 photolysis rate (J_{NO_2}). Chemical emission of NO_2 is also included in the model and is scaled as a function of J_{NO_2}. These emissions are added to the lowest model level, to simulate

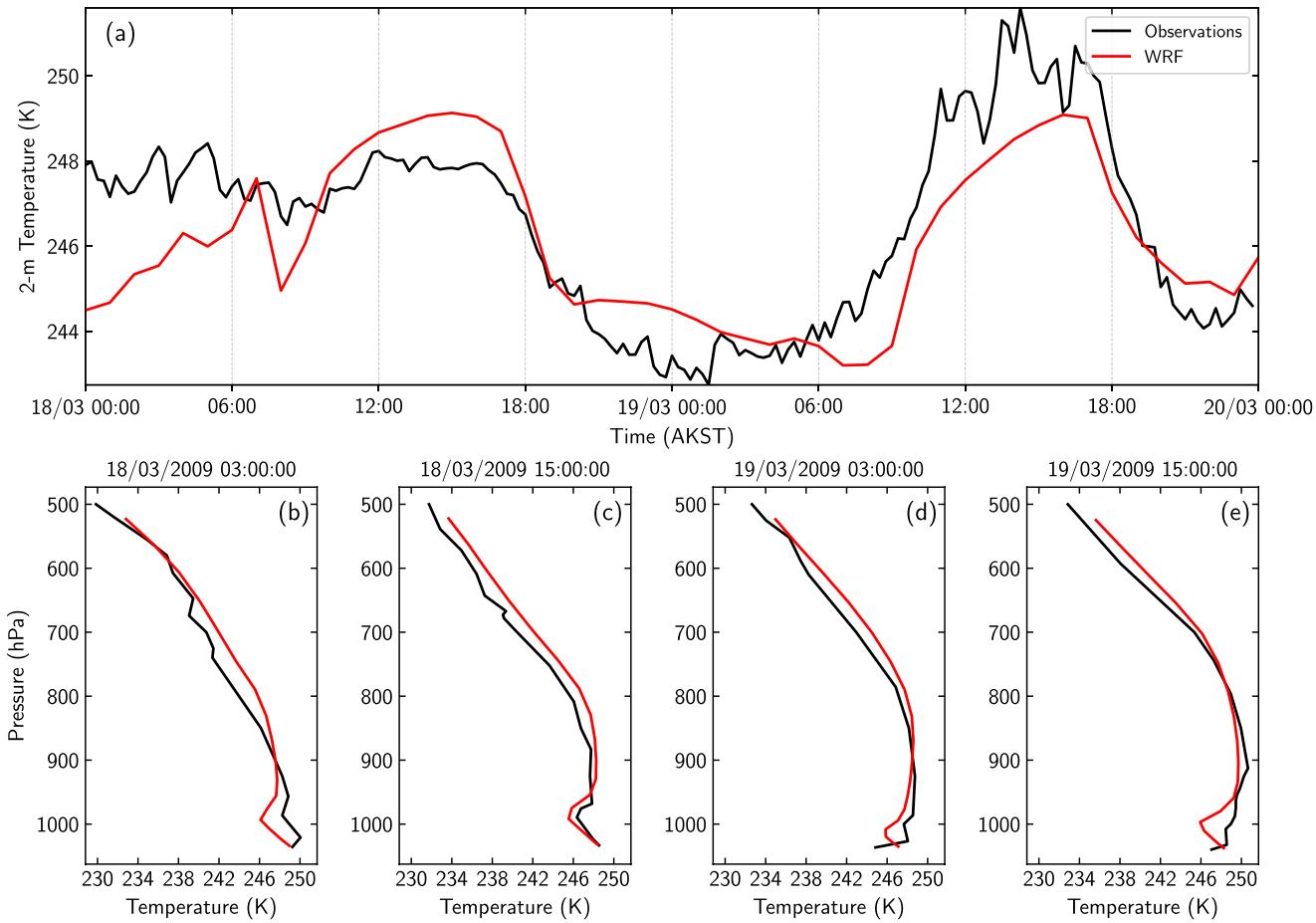


Figure 4. Temperature comparison between the WRF model (red) and measurements (black) at Utqiaġvik, Alaska during the simulation period. (a) 2-m temperature from WRF and surface measurements from OASIS. (b–e) Vertical temperature profiles from WRF and NOAA IGRA radiosondes released every 12 hr during the simulation period (dates and times are in Alaska standard time).

photochemical production from snow, and scaled to align with the NO_x levels measured during the simulation period. The 24-hr average NO_2 emission flux we use is 1.71×10^{13} molecules m^{-2} s^{-1}, in reasonable agreement with previous Arctic NO_x flux measurements (Honrath et al., 2002). All input data are provided on 15 min time resolution and the model is run using a 20-s time step.

5. Results and Discussion

We study the impact of halogen emissions on oxidation processes during OASIS by performing the following model runs: a reference simulation without halogen emissions from snow (NOSURF); a model run with surface snow emissions and recycling of halogens active (BASE); and several sensitivity runs (FIXO3, AERO, BLD). The model runs are summarized in Table 3 and are discussed in detail in the following section. In all model runs, we include heterogeneous chemistry on aerosols, which participates in active recycling of halogen species in all cases. We present the results and discussion in seven sub-sections. First, we present the meteorological conditions at the measurement site during the modeled period (Section 5.1), followed by an analysis of the NOSURF (Section 5.2) and BASE runs (Section 5.3). We discuss in detail the results of the sensitivity tests performed (Section 5.4), the influence of snow emissions on the vertical extent of halogen concentrations (Section 5.5) and a comparison of the snow emission fluxes with other estimates (Section 5.6). Finally, we analyze the impacts on boundary layer oxidation processes (Section 5.7).

Table 3
Description of the Model Runs Performed in This Study

Model run	Description
NOSURF	Run with halogen snowpack emission routines deactivated.
BASE	Run with halogen snowpack emission and recycling routines active.
FIXO3	BASE run + O_3 fixed to the observations.
AERO	BASE run + heterogeneous recycling efficiency on aerosols increased by a factor of 10.
BLD	BASE run + surface inversion height estimated using expression from Pollard et al. (1973).

5.1. Meteorological Conditions and Air Mass History

The measurements during OASIS were made approximately 5.5 km northeast of Utqiaġvik, Alaska, near the Arctic Ocean (Barret et al., 2011; Boylan et al., 2014; Helmig et al., 2012; Hornbrook et al., 2016; Liao, Huey, Tanner, et al., 2012; Liao et al., 2014; Villena et al., 2011). Figures 2a and 2b show the sea ice cover and lead information over Northern Alaska on 18 and 19 March 2009, respectively. Lead information is obtained from the dataset of Willmes and Heinemann (2015) who used thermal-infrared data retrieved from MODIS and applied a binary segmentation procedure to identify leads (Willmes & Heinemann, 2016). During March, the sample location was snow covered and the surrounding ocean largely covered by sea ice, typically reaching its annual maximum in spring. Sea ice leads are clearly visible during the simulation period north of Utqiaġvik, which are known to be important for inducing convective mixing that influences atmospheric chemistry (Moore et al., 2014; Simpson et al., 2017). Meteorological conditions, such as wind speed, wind direction and surface temperature, can also alter surface chemical concentrations via impacts on boundary layer dynamics. Winds on both days were recorded arriving from the northeast, over the Beaufort Sea, carrying clean air masses to the measurement site. During this period, wind speeds were moderate to weak (<5 m s^{-1}; Figure S4 in Supporting Information S1), lower than much of the campaign period, and surface temperatures were close to the March average. A strong low-level temperature inversion was also observed for the duration of these 2 days, indicating stable boundary layer conditions, which is likely to inhibit vertical mixing of species between the inversion layer top and the overlying atmosphere (Figure S5 in Supporting Information S1).

We use the regional meteorological model WRF (setup described in Section 4.2) to both drive the 1D model atmospheric physics and to understand the regional meteorological conditions during the sampling period. Simulated 2-m temperature and 10-m winds over Northern Alaska are shown in Figures 2c and 2d on 18 and 19 March 2009 (local noon) respectively. The wind direction from WRF on both days captures the northern/northeasterly winds measured at the site, as well as the weaker wind speeds on 19 March. This analysis allows us to next identify the origin for air arriving at the measurement site, using the Lagrangian particle dispersion model, FLEXPART-WRF (Brioude et al., 2013). FLEXPART-WRF is driven by the meteorological conditions simulated by WRF and is run in backward mode to simulate air mass histories for the modeled period. These simulations are performed by releasing a total of 100,000 air parcels at the time when Cl_2 maxima were observed for each day (10:00 a.m. and 6:00 p.m. local time for 18 and 19 March, respectively) and run backwards in time for 6 hr. Figures 2e and 2f, show the calculated surface (0–100 m) potential emission sensitivities (PES) near the measurement site. The PES indicates the air mass origin near the surface and represents the length of time the air mass is sensitive to surface emissions. In Figures 2e and 2f, we show that air masses on these days were unaffected by either the town of Utqiaġvik or Prudhoe Bay (southeast of Utqiaġvik, not shown on map). Transport of air masses over sea ice, including leads, may impact the halogen concentrations measured at the site. On both days, the PES shows (Figures 2e and 2f) that air passes over leads (Figures 2a and 2b) just before arrival at Utqiaġvik. Moore et al. (2014) showed that the rapid recovery of depleted mercury and ozone, which are both tied to the abundance of bromine, can be explained by lead-initiated convection bringing higher concentrations of Hg^0 and ozone from aloft. This also indicates that high concentrations of bromine in these air masses are likely diluted over leads during the induced convective mixing, as shown by Simpson et al. (2017). Due to the air mass origins and lead locations, and the relatively short lifetimes of Cl_2 and Br_2, our case is expected to be particularly sensitive to local snow emissions and so we assume that this provides the main source of Cl_2 and Br_2 for our case study (see Section 5.2).

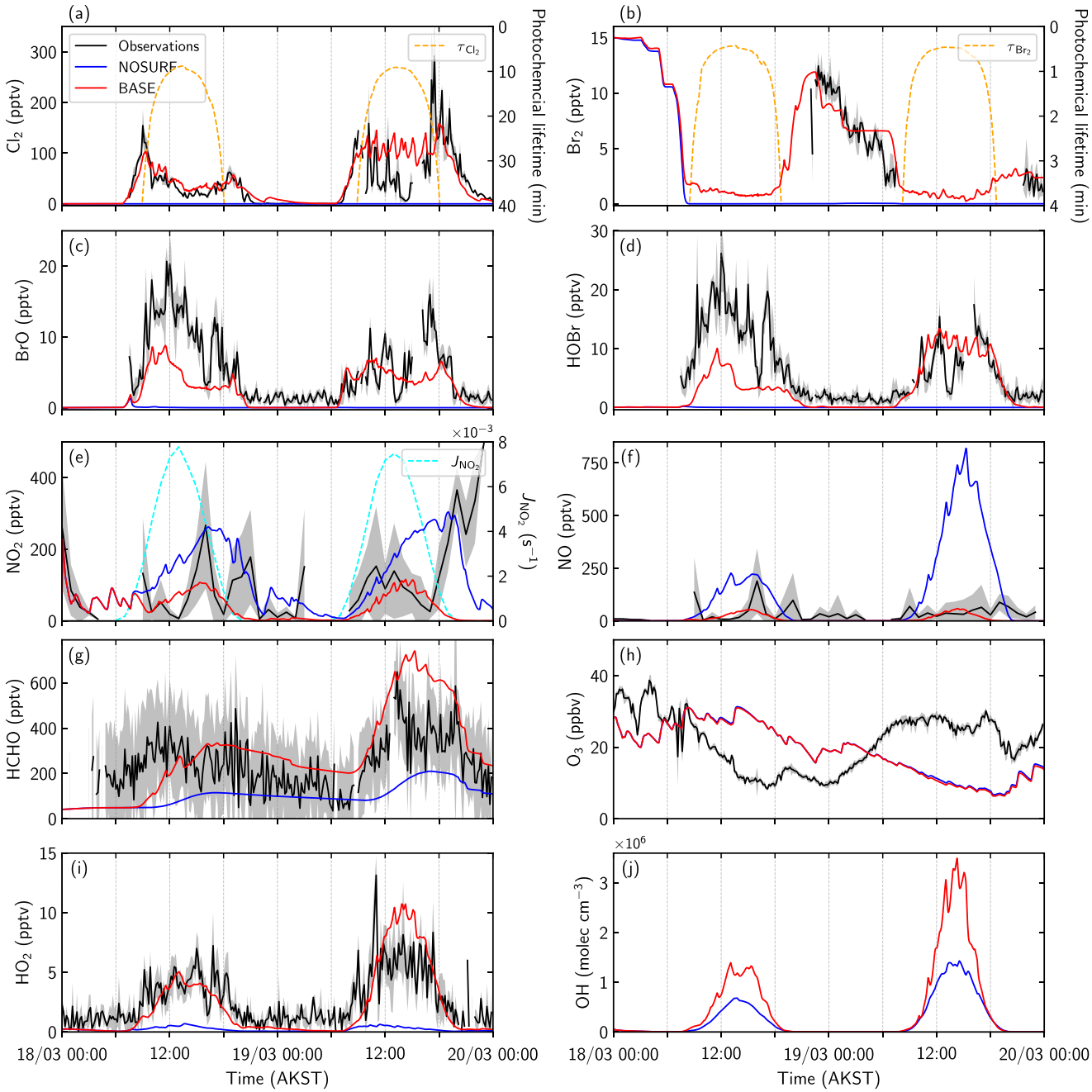


Figure 5. Model comparison with observations at 1.5 m above ground level during 18 and 19 March 2009. NOSURF (blue) and BASE (red) runs are compared with the 10-min averaged measurements (black). NO_x measurements are plotted as an hourly average. Gray shaded areas represent the standard deviation of the average from the instantaneous measurements. Photochemical lifetimes of Cl_2 (τ_{Cl_2}) and Br_2 (τ_{Br_2}) (orange) and the calculated photolysis rate of NO_2 (J_{NO_2}) (cyan) are also plotted.

5.2. Model Results Without Snow Emissions or Recycling

A model simulation without halogen emissions from snow or surface recycling (NOSURF) was first performed as a reference simulation. The results from this simulation are compared to measured species at 1.5 m AGL in Figure 5 (blue curve). The halogen species (Cl_2, BrO, and HOBr) in this simulation remain negligible for the duration of the simulation, with the exception of Br_2 which is initialized as described below, showing that additional sources of both chlorine and bromine are required to explain the observations. Surface Br_2 is initialized to the average midnight value (15 pptv) that was recorded during OASIS (Liao, Huey, Tanner, et al., 2012), which

fell rapidly to zero after 08:00 on the first day, indicative of photochemical loss. No significant levels of Br_2 after this period are modeled, suggesting that bromine recycling solely on aerosols is not efficient enough to replenish measured levels of Br_2 and other bromine species. Local snow emissions of Br_2 are therefore necessary to replenish bromine levels during the simulation period.

Surface measurements of both NO and NO_2 were higher than the background average (~82 pptv), reaching daytime peaks of close to 250 pptv and over 400 pptv at night on 19 March. These measurements were likely impacted by both local background NO_x emissions from snow (Honrath et al., 1999, 2002) and transient point sources. We filtered out the extreme elevated point sources of pollution (above 500 pptv), and use an hourly average of NO and NO_2 concentrations to smooth out sharp peaks arising from local point sources. The observations (Figures 5e and 5f) show some remaining sharp peaks of NO_x on both days, likely caused by these local emission sources, which are difficult to estimate. In addition, a large increase of NO_2 on the evening of 19 March was recorded, corresponding with a change of wind direction and air mass, bringing air from more polluted regions to the measurement site. Stable conditions and low wind speeds may have also facilitated the build-up of higher NO_x concentrations near the surface on these 2 days. The impact of these local point sources, and of advected polluted air masses, are therefore difficult to simulate in the model to represent the true NO_x concentrations observed at the measurement site. Modeled values reach and even exceed the measured daytime peaks, with a large overestimation in NO on day 2, before falling to lower than 100 pptv at night. The low concentration of modeled halogens would certainly contribute to the overestimation of NO_x concentrations via halogen oxide limited reactions with NO and NO_2. Changes in the surface ozone levels over the 2 days are not fully captured by either the NOSURF or BASE simulations. This is possibly due to sea ice leads and convective mixing of ozone down from the free troposphere to the surface. The model currently does not account for the impact of sea ice leads on convective mixing of air masses, and would require further testing to include. Finally, we find a general underestimation of both HCHO and HO_2 levels, indicating missing oxidants and oxidation chemistry, and a predicted midday OH concentration between 0.7×10^6 and 1.5×10^6 molecules cm^{-3} for the 2 days.

5.3. Model Results With Halogen Emissions From Snow and Surface Recycling

When snow and recycling emissions of halogens are active (BASE run), we obtain much better agreement with the measured surface mixing ratios compared to the NOSURF run. Measured Cl_2 levels reached up to 150 and 300 pptv on 18 and 19 March 2009, respectively (10 min average). Figure 5 (red curve) shows the model performs well, capturing both the timing and intensity of the morning and late afternoon Cl_2 peaks on the first day, with some discrepancies on day 2. Early morning increase of Cl_2 was recorded after sunrise, suggesting a photochemical production mechanism, which is captured by the model on both days. Daytime levels of modeled Cl_2 on day 2 are overpredicted, by up to 100 pptv, with the difference possibly explained by weak vertical mixing and a shallow daytime boundary layer. The effects of this on surface chemical concentrations are discussed in more detail in Section 5.5. Nighttime Cl_2 mixing ratios fall to near-zero levels in the model, which is consistent with the measurements on both days. Our model results show that the nighttime (20:00–06:00) reduction of Cl_2 at 1.5 m is largely explained by depositional loss to the ground (see Section 5.5). Together, vertical transport and deposition represent the dominant nighttime loss processes (~94%) for Cl_2 at 1.5 m. Heterogeneous uptake of Cl_2 on aerosols and reaction with bromide has also been suggested as a potential Cl_2 sink (and a source of BrCl) (Hu et al., 1995; McNamara et al., 2020; Wang & Pratt, 2017). We find that the reaction of Cl_2 with bromide on aerosols accounts for nearly 5% of nighttime removal of Cl_2 at 1.5 m, which comprises the majority (95%) of the nighttime chemical loss for Cl_2.

Modeled bromine species (Br_2, BrO, and HOBr; Figures 5b–5d, respectively) are also in close agreement with the measurements, with a slight underestimation of BrO and HOBr on day 1. Daytime measurements of Br_2 on these 2 days are missing due to unstable background Br_2 measurements that led to observations below the detection limit (2.0 pptv) (Liao, Huey, Tanner, et al., 2012). We find that modeled daytime levels of Br_2 are close to this 2 pptv detection limit, due its very fast photochemical loss. At night, we find an accumulation of the photolabile Br_2, via the surface recycling mechanism, which provides reactive bromine for the following day. This is consistent with the average diurnal profile measured for Br_2 during OASIS (Liao, Huey, Tanner, et al., 2012), as well as other Arctic measurement campaigns during spring (McNamara et al., 2020; Wang et al., 2019). Modeled BrO and HOBr diurnal profiles are also in agreement with the observations, with peaks at noon on the first day, indicative of production via Br atoms, and near zero at night. On day 2, a second peak for both BrO and HOBr

is recorded in the late afternoon, coinciding with the evening peak of Cl_2. This suggests that the second peak in halogen species could possibly be due to a change in the boundary layer meteorology (e.g., collapse of the boundary layer) rather than chemical production.

The model captures the general trend of NO_x (Figures 5e and 5f) and we obtain better agreement with the observations in the BASE run, however, the model does not capture some peaks which may be due to advection of more polluted air masses (e.g., evening of 19 March) or transient point sources. Simulated NO_x levels are highly affected by the presence of halogen emissions, with both NO and NO_2 levels reduced in the BASE run compared to NOSURF. Halogens can react with NO_x to produce halogen nitrites and nitrates (e.g., $ClNO_2$, $ClONO_2$, $BrONO_2$), which act as an important reservoir to sustain reactive halogen chemistry. These species can release halogens back into the atmosphere either directly via photolytic destruction, or by chemical reactions on aerosols and surface snow. O_3 levels in the BASE run also show a steady decline over the 2 days, with O_3 changes dominated by vertical mixing and deposition to the ground in our particular simulation period (Figure 5h). Modeled HCHO (Figure 5g) and HO_2 (Figure 5i) are also in better agreement with the observations following the addition of halogen emissions. We find an increase in the daytime HO_x ($HO_x = OH + HO_2$) levels by roughly 20–30 times compared to the NOSURF run, indicating much more active HO_x chemistry, which can be attributed to halogen chemistry. Overall, we show that halogen emissions from snow and snow-surface recycling are necessary to reproduce surface concentrations of several key species measured during OASIS, with a considerable impact on HO_x concentrations and oxidative chemistry.

5.4. Model Sensitivity Runs

We investigate the effects of different model uncertainties on surface chemical concentrations by performing three sensitivity tests. The aim of these runs is to explore uncertainties in both the chemical and dynamical mechanisms in our model and their associated impacts on surface concentrations. Specifically, we test whether changes in the modeled ozone concentration, halogen recycling on aerosols, or boundary layer dynamics impact the conclusions drawn from this modeling study. Descriptions of the runs performed are included in Table 3 and are summarized here, followed by a discussion of the results compared with the surface observations (Figure 6).

1. **FIXO3**: We first address the impact of ozone on halogen concentrations by fixing the modeled ozone to the measurements within the boundary layer (Figure 6, dashed green curve). Bromine levels in this run are greatly affected by the change in ozone availability due to the reaction with Br atoms (R2). On 18 March, BrO and HOBr are both underestimated in this run compared to the observations, followed by an overestimation on 19 March (when there was more ozone available). Nighttime Br_2 levels are underestimated by ~10 pptv compared to the observations and BASE run, with this difference likely explained by the lower levels of BrO on day 1, resulting in less $BrONO_2$ formation and recycling to re-form Br_2. The daytime HO_2 concentration on day 2 is approximately 68% lower than the BASE run, due to increased BrO levels and subsequent loss via reaction (R5). The results from this run point to potential inaccuracies in the emission parameterizations of bromine, uncertainties in the downward mixing of ozone in the model from above the boundary layer, or, to the missing treatment of advected air masses, all of which require further exploration and testing
2. **AERO**: To test whether heterogeneous recycling on aerosols could contribute a significant source of halogens, we increase the heterogeneous reactive uptake coefficients for Cl_2, Br_2, and BrCl formation reactions by a factor of 10 (Figure 6, dashed purple curve). This test fails to show a significant increase in the halogen concentrations at the surface, indicating that recycling on aerosols contribute only a minor source of reactive halogens at 1.5 m. Interestingly, nighttime Br_2 levels decreased by up to 5 pptv when compared to the BASE run, caused by lower $BrONO_2$ levels (~25% reduction) as it was more efficiently recycled on aerosols. We also evaluate the difference in the vertical distribution of halogens between the AERO and BASE run (Figure S6 in Supporting Information S1). The modeled vertical distribution of halogens in the BASE run is discussed in detail in Section 5.5. We find differences of less than 10 pptv between halogens in the AERO run and the BASE run within the lowest 50 m of the model, and see no differences above this height. Specifically, we find an increase in Cl_2 concentrations of several pptv in the AERO run and a small decrease for each modeled bromine species
3. **BLD**: We explore uncertainties in the boundary layer dynamics by testing a different expression to calculate the SIH from the meteorological measurements (Figure 6, dashed blue curve). The expression used in this run

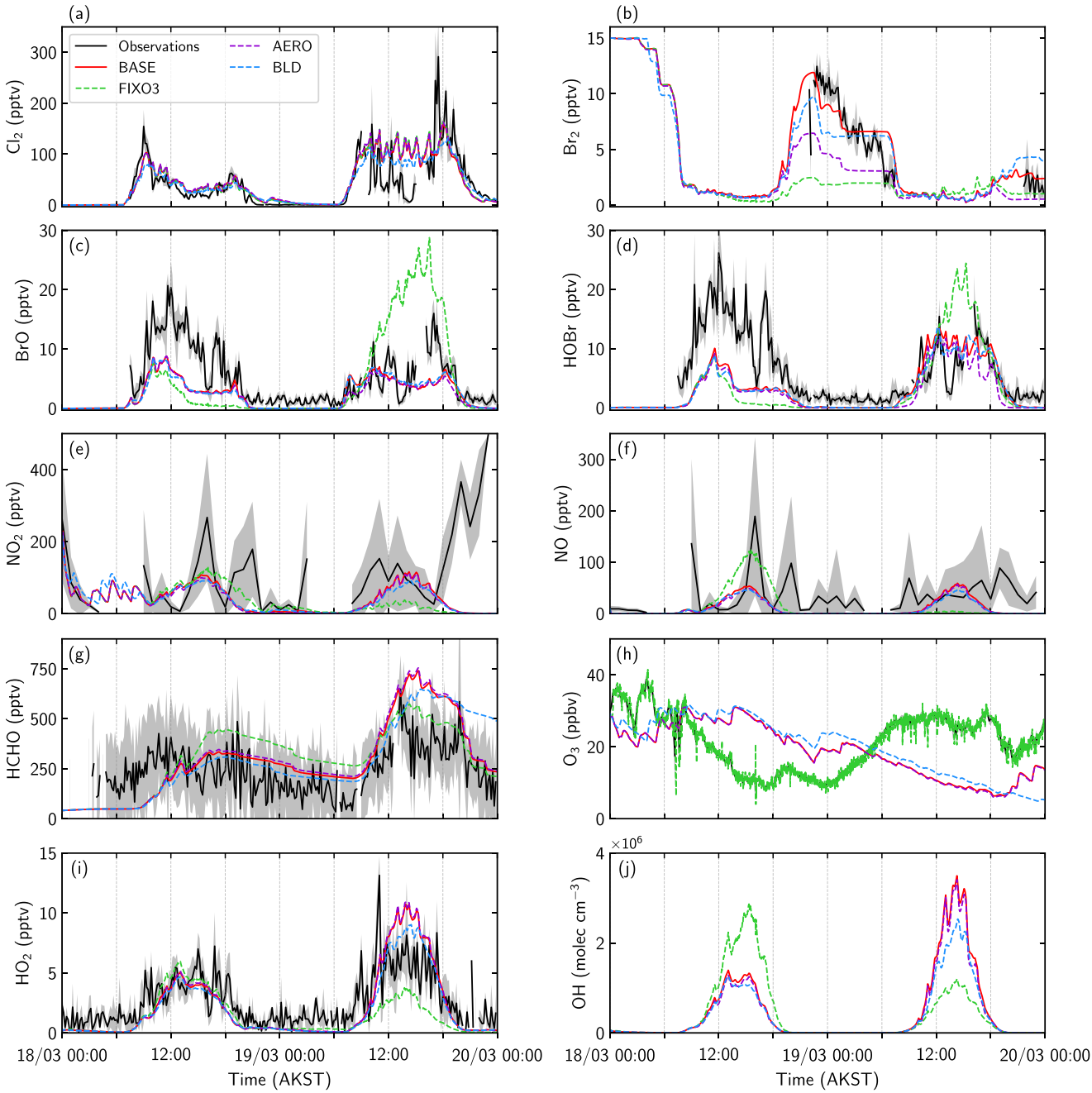


Figure 6. Model comparison of sensitivity runs with observations at 1.5 m above ground level during 18 and 19 March 2009. BASE (red), FIXO3 (dashed green), AERO (dashed purple) and BLD (dashed blue) runs are compared with the 10-min averaged measurements (black). NO_x measurements are plotted as an hourly average. Gray shaded areas represent the standard deviation of the average from the instantaneous measurements.

(Equation 6) was originally developed for a stable mixed layer over the ocean by Pollard et al. (1973), and was found to also be applicable to the South Pole by Neff et al. (2008)

$$\mathrm{SIH} = 1.2u_*(fN_B)^{-0.5} \tag{6}$$

$$N_B = \sqrt{\frac{g}{T}\frac{\partial\theta}{\partial z}} \tag{7}$$

where u_* is the measured friction velocity, f is the Coriolis parameter (equal to 1.38×10^4 at the latitude of the study site), N_B is the Brunt-Vaisala frequency, g is the acceleration due to gravity, T is the absolute temperature and $\partial\theta/\partial z$ is the potential temperature gradient. This results in a SIH which is several meters greater than previously used for the BASE run (Figure S5 in Supporting Information S1), leading to some key differences in the modeled chemical species. Most notably, we see a reduction in daytime Cl_2 levels at 1.5 m, by up to 60 pptv, on day 2 compared to the BASE run due to an increased SIH. This shows how sensitive surface concentrations can be to small changes in the boundary layer conditions, with significant uncertainties in vertical transport near the snow surface and lower atmosphere. This is discussed in more detail in Section 5.5.

In summary, the sensitivity runs performed here do not significantly improve model agreement with the observations. However, these sensitivity tests show that modeled surface concentrations are influenced by a number of parameters, which require better understanding of specific processes in order to constrain halogen emissions. Changes in ozone and boundary layer dynamics (vertical mixing) had the largest impacts on halogen concentrations, as well as influencing surface NO_x and HO_x levels. We find that uncertainties in heterogeneous reactions on aerosols do not explain the underestimation of BrO and HOBr on day 1, and represent only a minor source contribution of halogens in our model case. Additional studies designed to investigate these processes and reduce known uncertainties for the Arctic region are needed to further evaluate the source contributions of halogens from snow.

5.5. Vertical Influence of Snow Emissions and Recycling on Halogens

In this section, we use the BASE run to understand the vertical distributions of Cl_2 and Br_2 (Figures 7a and 7b, respectively). No vertically resolved measurements were available for either species, therefore, no direct comparison can be made to the model results. We find that the majority of modeled Cl_2 (approximately 97%) is confined to the lowest 15 m of the atmosphere and rapidly decreases with altitude. This implies highly active chlorine chemistry at the surface. Very little Cl_2 is present above 15 m, indicating a strong vertical gradient in chemical reactivities, with the vertical distribution of Cl_2 influenced by the height of the surface inversion. During the campaign, the surface layer height ranged from as low as a few meters up to several hundreds of meters and was estimated to be very shallow (<50 m) during the simulation period (Boylan et al., 2014). Low-level temperature inversions and shallow boundary layers are a common phenomena in cold polar regions and are frequently characterized by stable conditions and low wind speeds. Typically, solar heating of the surface generates a turbulent well-mixed daytime boundary layer, creating a larger volume in which chemical species can be distributed. This simultaneously increases the vertical transport of species away from the surface and results in decreasing concentrations of chemical species that would otherwise build up near the surface. The diurnal evolution of the surface layer can be seen following this behavior on the first day but not on the second. We are therefore able to capture the daytime reduction in surface Cl_2 levels on day 1, following the morning peak, but overestimate Cl_2 levels on day 2. This high daytime Cl_2 concentration is simulated when the wind speed and estimated SIH were very low (<1 m s^{-1} and <10 m, respectively), confining Cl_2 to a very shallow layer close to the surface. The BLD sensitivity test also shows similar behavior of the surface layer on the second day, however, estimated a SIH several meters higher during the day, resulting in a reduction of Cl_2 at this time (Figures S5 and S7 in Supporting Information S1). Differences in the SIH estimates between Equations 5 and 6 are discussed in detail by Boylan et al. (2014), but further evaluation is beyond the scope of this study.

The modeled vertical distribution of Br_2, presented in Figure 7b, shows that Br_2 is present up to and above the SIH during the simulation. During sunlit hours, Br_2 is found only within the first few meters of the model, whereas at night, Br_2 is more abundant (approx. 10 pptv) reaching up to 40 m in height. Previous studies have examined the vertical distribution of bromine in the Arctic via surface-based measurements of BrO (Peterson et al., 2015; Simpson et al., 2017). Peterson et al. (2015) found that the percentage of BrO within the lower troposphere (<200 m) was highly dependent on atmospheric stability. During stable conditions, higher BrO mixing ratios were measured close to the surface, with less BrO distributed within the lower troposphere, compared to unstable conditions which were associated with more vertically distributed BrO events. Simpson et al. (2017) also observed shallow layer events of BrO during stable conditions, and during lead opening events, found that BrO was lofted above the surface via lead-induced convective mixing. Air that had traveled over sea ice, arriving at the measurement site with very low ozone representing ODE conditions and very active bromine chemistry, are not specifically investigated here. However, there are some similarities between what we investigate regarding

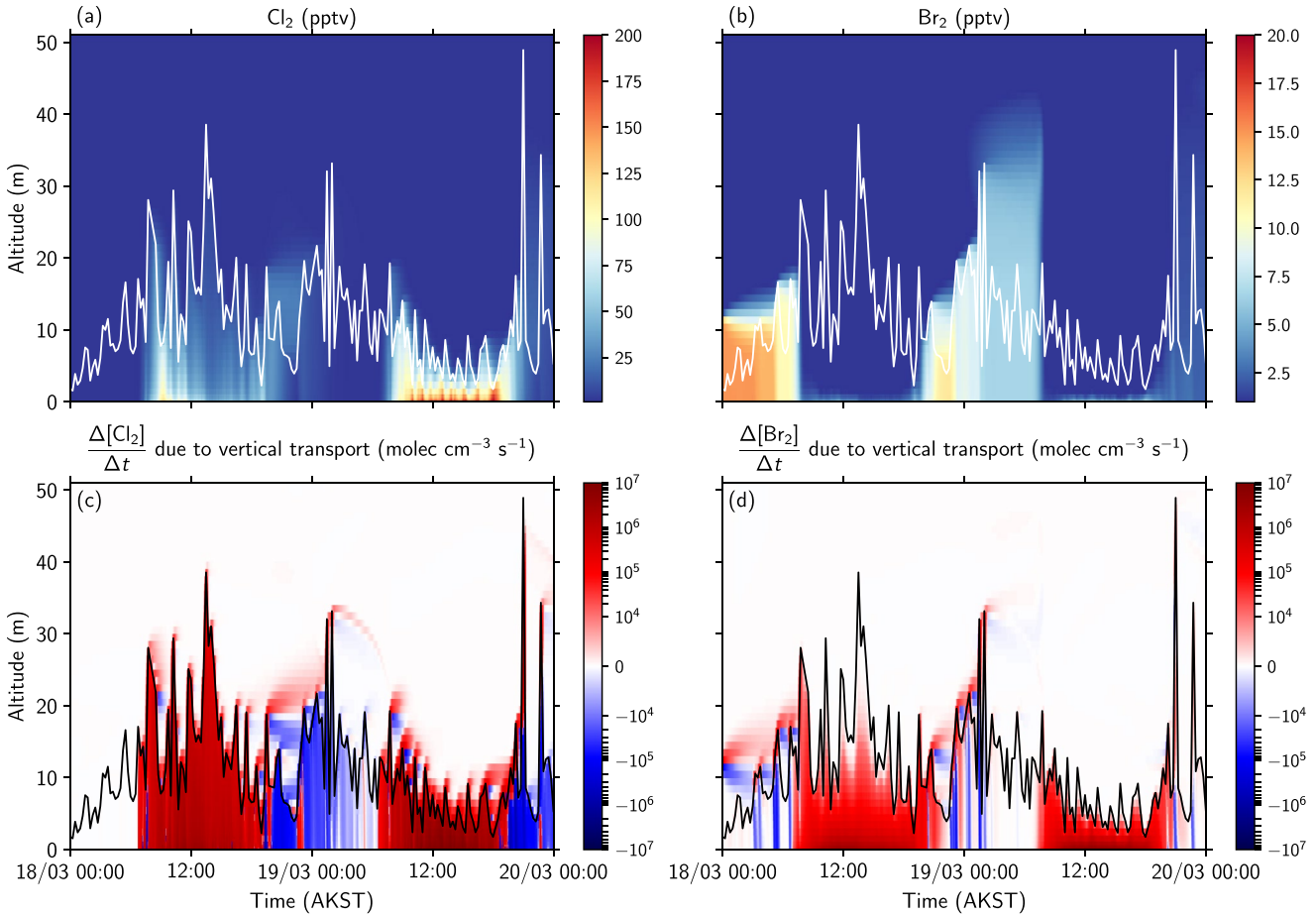


Figure 7. Modeled vertical distributions of (a) Cl_2 and (b) Br_2 during 18 and 19 March 2009 in the BASE run. White trace indicates the model prescribed SIH. Modeled concentration change of (c) Cl_2 and (d) Br_2 due to vertical transport and deposition with respect to time. Black trace indicates the prescribed SIH. Positive values represent upward transport and negative values indicate downward transport.

land-based snow emissions of both bromine and chlorine and what is known about bromine activation from snow on sea ice, where atmospheric boundary layer stability is similar. During the simulation, we find that both BrO and HOBr are present within and above the SIH, reaching heights of up to 40 m during the day (Figure S8 in Supporting Information S1). This is in agreement with the findings of Peterson et al. (2015), as the stable conditions recorded between 18 and 19 March would suggest a shallow layer event of BrO. However, it is also important to note that the air masses arriving at the site could have possibly experienced some lead-induced convective mixing (see Figure 2), which would mix bromine to higher altitudes and this is not considered in the model.

In Figures 7c and 7d, we plot the changes in concentration of Cl_2 and Br_2 due to transport and deposition, respectively. The change in both Cl_2 and Br_2 concentrations, due to vertical transport, is highest during the day following release from snow and transport into the atmosphere. During the night, Cl_2 is mainly transported downward to the surface and lost via deposition to the ground. Deposition in the model is calculated using an approach of molecular collisions with the ground and applying a non-reactive uptake probability (α; Tuite et al., 2021). This allows us to calculate deposition of different species without prescribing a deposition velocity. For Cl_2, we set $\alpha = 5 \times 10^{-5}$, following the lower limit recommendation of Burkholder et al. (2019). On 19 March, transport of Cl_2 is clearly limited by the height of the inversion layer, with Cl_2 transport not exceeding more than 15 m altitude, thereby concentrating Cl_2 at the surface. Figure 7d shows that the upward transport of Br_2 is at its maximum during the day on 18 and 19 March. Daytime Br_2 concentrations are confined to the first few meters above ground, indicating that daytime Br_2 is lost via its fast photolytic destruction. Vertically resolved measurements of halogens above the Arctic snow surface are highly desirable for further model evaluation and development.

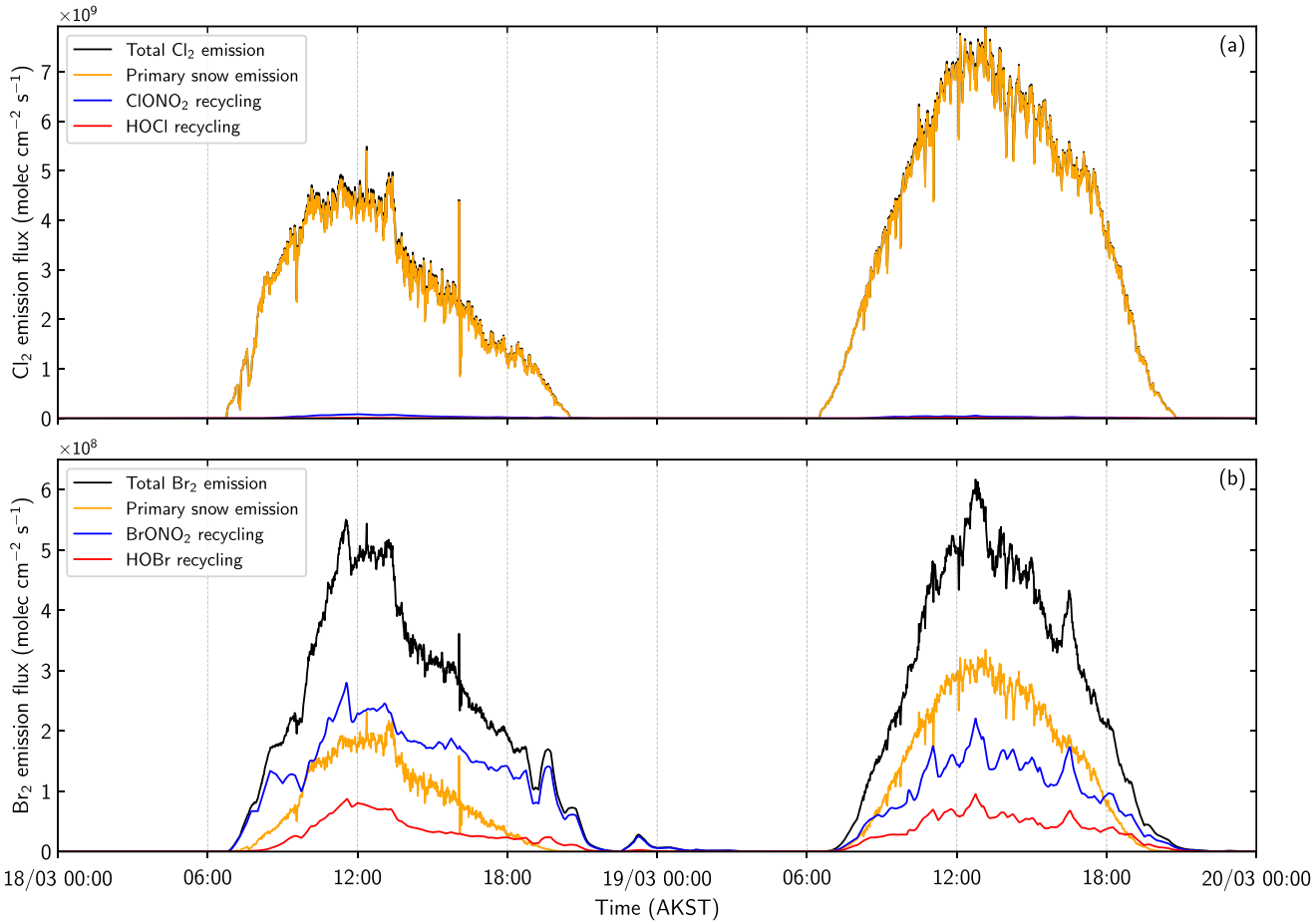


Figure 8. Snow emission and recycling fluxes of (a) Cl_2 and (b) Br_2 in the BASE run. The total emission flux (black) for each species is plotted together with the primary snow emission flux (orange) and recycling fluxes of $XONO_2$ (blue) and HOX (red), where X = Cl and Br.

5.6. Modeled Halogen Snow Emission Fluxes Compared to Previous Estimates

Here, we compare the surface emission fluxes of Cl_2 and Br_2 estimated in this work to previous flux estimates. The model emission flux contributions of Cl_2 and Br_2 are shown in Figures 8a and 8b, respectively. Our modeled emissions of both Cl_2 and Br_2 peak at solar noon on each day, coinciding with increased radiation at the snow surface, before falling to zero at night. The peak fluxes are similar to previously reported halogen emission fluxes measured from the Arctic snowpack (Custard et al., 2017), while the exact timing of emissions differs. During February 2014, snowpack flux estimates of Arctic Br_2 and Cl_2 were calculated, based on vertical gradient measurements, for the first time near Utqiaġvik. Estimates of these fluxes ranged between $0.7–12 \times 10^8$ and $0.02–1.4 \times 10^9$ molecules cm^{-2} s^{-1} for Br_2 and Cl_2, respectively. We modeled midday fluxes for Cl_2 of 4.3×10^9 and 7.2×10^9 molecules cm^{-2} s^{-1} for 18 and 19 March, respectively, with the primary photochemical snow emission mechanism the main contributor to Cl_2 emissions. This is several times higher than the values reported by Custard et al. (2017). This may in part be explained by increased available sunlight during March compared to February (when the flux measurements were made), enhancing halogen production. Additionally, ambient concentrations of Cl_2 were much lower in February 2014 than those measured in March 2009, with daytime values ranging between 5 and 20 pptv in February 2014 and 59 pptv for the simulation period. Both of these reasons would suggest higher snow emission fluxes of halogens between 18 and 19 March 2009 than estimated previously.

During the OASIS campaign, Liao et al. (2014) estimated an average peak production of Cl_2 of 2.2×10^6 molecules cm^{-3} s^{-1} using 0D box modeling. Assuming a 15 m mixing layer, this corresponds to an average emission flux of 3.3×10^9 molecules cm^{-2} s^{-1}. This is slightly lower than the value we report here, which is likely due to

our focus on an extremely high Cl_2 event during the campaign. Similarly, Wang and Pratt (2017) conducted a 0D box modeling study to simulate halogen snowpack production during March 2012 near Utqiaġvik. A peak Cl_2 production rate of 2.9−3.2 × 10^8 molecules cm^{-2} s^{-1} was reported (assuming a 10 m effective mixing height), with ambient Cl_2 concentrations ranging between 0 and 20 pptv for the modeled periods. The lower ambient Cl_2 concentrations during March 2012 suggest that solar radiation is not the driving factor for differences between Cl_2 emission fluxes during February and March. Other factors such as atmospheric stability, vertical mixing, and snowpack chemistry are also likely to play a role in controlling molecular halogen emission fluxes from snow. Production of Cl_2 via snow surface recycling of HOCl and $ClONO_2$ was also minimal over the 2 days, with almost no production of Cl_2 at night, which explains the difference in the nighttime concentrations of Cl_2 and Br_2. There are uncertainties to the efficiency of this recycling (see Section 3.2), however, sensitivity tests showed no significant increase in Cl_2 when the recycling efficiency of these species was increased (Figure S2 in Supporting Information S1).

Figure 8b shows the modeled Br_2 emission fluxes, with midday values calculated at 4.9 × 10^8 and 5.0 × 10^8 molecules cm^{-2} s^{-1} for 18 and 19 March, respectively. These are in close agreement with the range reported by Custard et al. (2017) and are higher than those modeled by Wang and Pratt (2017) of 2.1 × 10^8 and 3.5 × 10^6 molecules cm^{-2} s^{-1} for 15 March and 24 March 2012 respectively. Both primary photochemical and snow recycling emissions of Br_2 are important production mechanisms and contribute significantly to the total Br_2 emission flux. Surface recycling of $BrONO_2$ is the main source of Br_2 on day 1, highlighting the influence of NO_x on bromine chemistry. This mechanism drives the accumulation of Br_2 at night, as this emission source remains significant later into the evening on day 1 compared to the primary snow emission, which falls to zero after sunset. Previous box modeling studies have shown that even under low NO_x levels (<100 pptv), formation of $BrONO_2$ is significant (Liao, Huey, Tanner, et al., 2012; Thomas et al., 2012; Wang & Pratt, 2017), and under high NO_x levels (>700 pptv) formation of both BrO and HOBr are suppressed, whereas the rate of $BrONO_2$ formation remained largely unaffected (Custard et al., 2015). Due to the difficulty of measuring $BrONO_2$, no measurements have yet been reported in the Arctic to the best of our knowledge. Future work remains to compare the partitioning of HOBr and $BrONO_2$ under different NO_x conditions.

5.7. Boundary Layer VOC Oxidation Processes

We have shown (in Section 5.3) that with the addition of halogen emissions (BASE run), we obtain good agreement with the measured HO_2 concentration at the surface and predict an increase in OH (Figure 5). To further understand the links between halogens, HO_x cycling and oxidative chemistry, we analyze the major HO_x production and loss reactions, as well as VOC chemical lifetimes with respect to OH and Cl. First, we compare the difference in modeled HO_x concentrations between the NOSURF and BASE runs, as well as the change in partitioning of OH/HO_2 between the two runs.

Figure 9a shows the modeled HO_x and Cl atom concentrations in the NOSURF and BASE runs at 1.5 m AGL. We see a clear impact of halogens on surface HO_x concentrations, with up to a 30 times increase at the surface when the halogen snow and recycling emissions are active. This increase is largest within the daytime surface layer, coinciding with the high levels of simulated chlorine atoms, and is shown in Figure 9b as a ratio of HO_x between the BASE and NOSURF runs. Modeled Cl atom concentration at noon is higher than the average concentration predicted during the campaign of 2.0 × 10^5 atoms cm^{-3} (Liao et al., 2014). We calculate values of 2.9 × 10^5 and 1.1 × 10^6 atoms cm^{-3} for 18 and 19 March at noon, respectively. Our higher values can partly be explained by the overestimation of modeled Cl_2 on day 2, as well as the higher Cl_2 levels observed during this period compared to the campaign average Cl_2 levels.

Figure 9c shows the calculated OH/HO_2 ratio at 1.5 m AGL in the NOSURF and BASE model runs. We find a significant shift in the OH/HO_2 ratio toward HO_2 in our BASE run following the addition of halogen emissions compared to the NOSURF run. This difference is largest during the day, within the lowest 40 m of the atmosphere, with up to an order of magnitude difference, as shown in Figure 9d. This shift toward HO_2 in the BASE run can be explained by two main reasons. First, with the chlorine sources active in the BASE run, HO_2 formation via Cl-mediated VOC oxidation is greatly increased, skewing the ratio toward HO_2. This is in support of previous studies, which have suggested that HO_2 can be increased by the presence of chlorine, shifting the OH/HO_2 ratio significantly toward HO_2 (Piot & von Glasow, 2009; Rudolph et al., 1999; Thompson et al., 2015). Second, as the model was not constrained to any observations, the addition of halogen sources had a significant impact

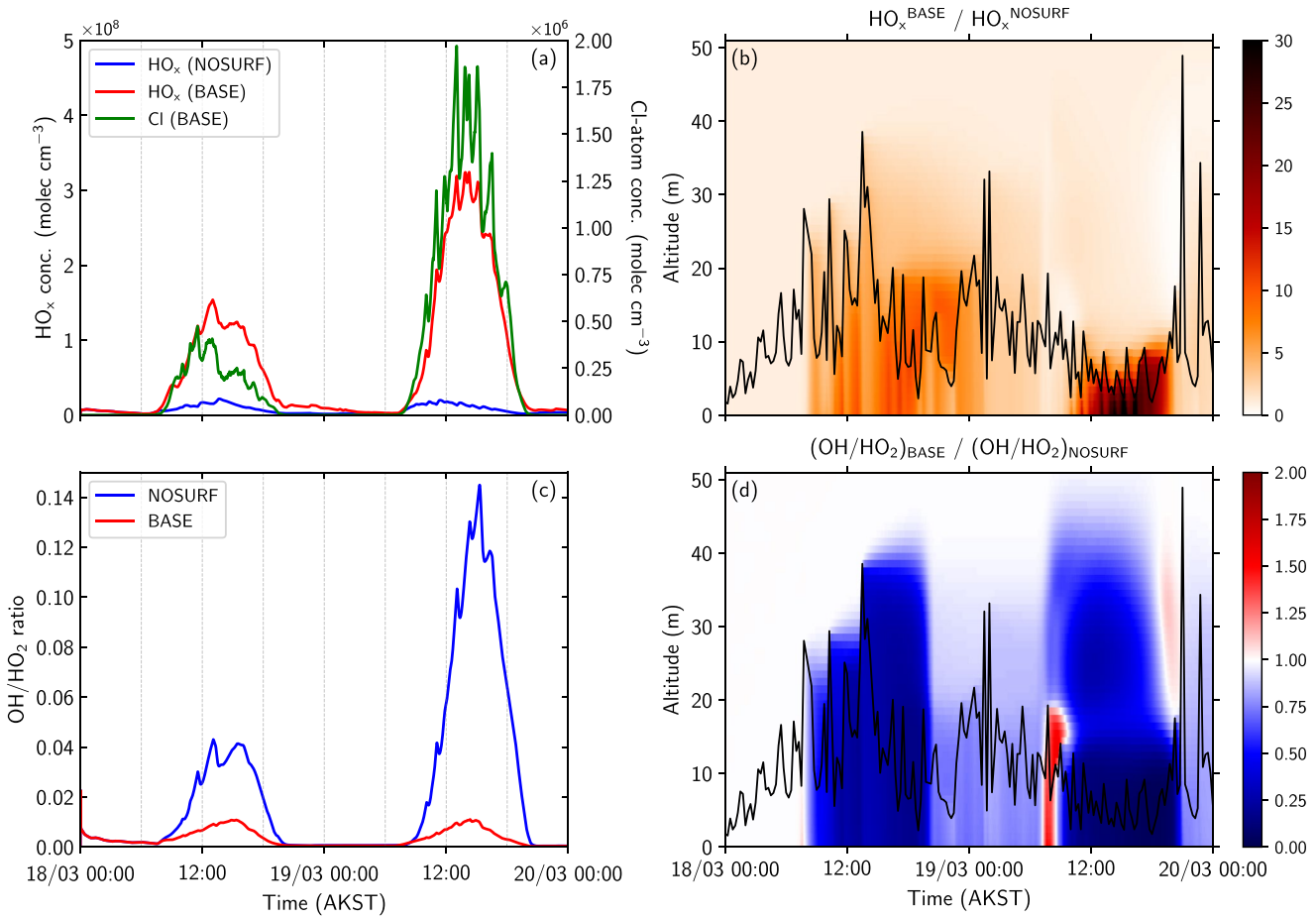


Figure 9. (a) Modeled HO_x concentrations at 1.5 m above ground level in the NOSURF (blue) and BASE (red) runs and Cl-atom concentration (green). (b) HO_x concentration in the BASE run divided by the HO_x concentration in the NOSURF run as a function of altitude. (c) OH/HO_2 ratio at 1.5 m above ground level in the NOSURF (blue) and BASE runs (red). (d) OH/HO_2 ratio in the BASE run divided by the OH/HO_2 ratio in the NOSURF run as a function of altitude.

on the NO_x concentrations. Surface NO_x levels in the NOSURF run were several times greater than the BASE run, which greatly impacted OH formation. Thomas et al. (2012) showed that modeled surface concentrations of OH double with the inclusion of snowpack NO_x sources and bromine chemistry. This was mainly driven by the NO + HO_2 reaction under conditions where the halogen concentrations were significantly lower than those measured at Utqiaġvik during OASIS. In order to further understand HO_x cycling in our model, we analyze the major production and loss reactions of both OH and HO_2.

5.7.1. HO_x Chemical Budget

The main HO_x production and loss reactions at two heights (1.5 and 50.5 m) above the snow are shown in Figure 10. A clear chemical reactivity gradient is shown, with rates at 1.5 m approximately an order of magnitude greater than at 50.5 m, due to increased HO_x and Cl atom concentrations in the lower atmosphere. The principal OH production source in the model is the HO_2 recycling reaction with NO, at both the surface and above the boundary layer at 50.5 m AGL. Halogen-influenced OH production is clearly shown at 1.5 m, accounting for almost a quarter of surface OH production, with photolysis of HOBr (R6) contributing 14% and reactions involving chlorine comprising nearly 10%. This is a significant direct impact of snow-sourced halogens on the OH concentration. Snow emissions of other species, such as nitrous acid (HONO) and hydrogen peroxide (H_2O_2), could also be important sources of OH which may not be fully represented by our simulations due to missing snow emissions of these species in our model runs. At 50.5 m, modeled halogen concentrations are low with limited contribution to OH production at this height. Reaction between ozone and HO_2 is the second most important pathway for OH production at this height and is particularly important as it continues to convert HO_2 to OH

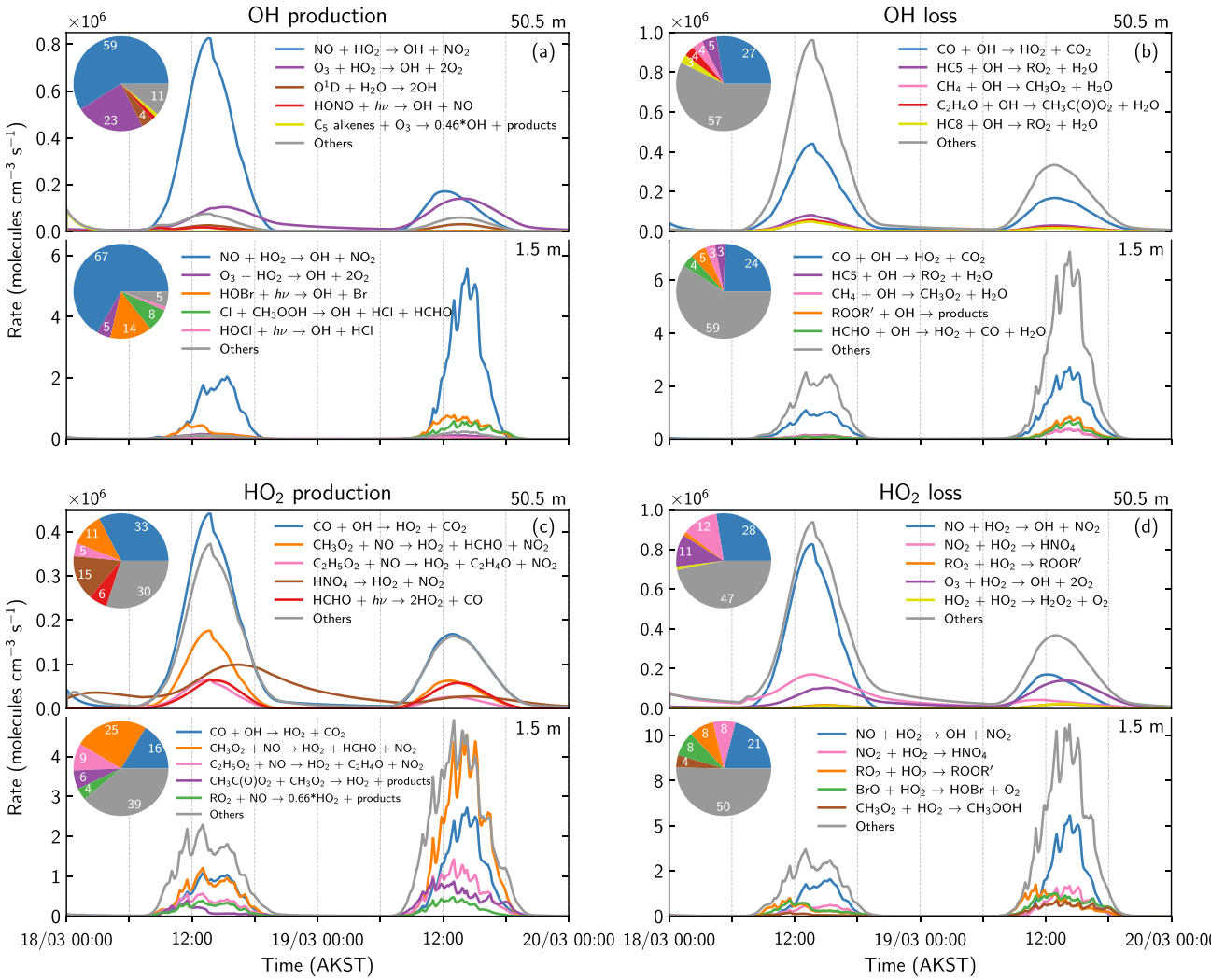


Figure 10. BASE simulation modeled (a) OH production (b) OH loss (c) HO_2 production, and (d) HO_2 loss each at 1.5 and 50.5 m above the snow surface. The five largest contributing reactions are shown for each with the percentage contributions shown as a pie chart.

for several hours after sunset. OH is lost via a multitude of reactions with organics, which can both recycle OH back into HO_2 and act as a source of CH_3O_2 and RO_2. Mainly, OH loss is dominated by the reaction with CO, accounting for approximately a quarter of OH loss at both heights, which is also an important source of HO_2.

At 1.5 m, the main HO_2 production reaction is the CH_3O_2 + NO reaction (25%), followed by CO + OH (16%). CH_3O_2 is formed following oxidation of VOCs and methane by OH and Cl, with the rate constant of Cl + CH_4 roughly an order of magnitude greater than OH + CH_4. Figure 11 shows the major production reactions of CH_3O_2 in our BASE run, with Cl + CH_4 responsible for almost two-thirds (64%) of surface CH_3O_2 production, whereas OH + CH_4 accounts for only 5%. At 50.5 m above the surface, production via Cl + CH_4 is negligible due to the low abundance of Cl atoms. Therefore, we can determine that snow emissions of chlorine drive the increase of surface HO_2 levels via CH_3O_2 formation. Consequently, this reaction cycle can also accelerate bromine recycling and ozone depletion, via (R5), linking together the chlorine and bromine chemical cycles. This effect is seen at 1.5 m, with BrO constituting 8% of HO_2 loss, with minimal contribution at 50.5 m.

In summary, it can be clearly seen that halogen emissions from snow make a significant contribution to HO_x production and loss reactions close to the surface. Chlorine and bromine chemical cycles are linked via peroxy radical formation, enhancing HO_x chemistry within the boundary layer, which can significantly impact VOC reactivity and lifetimes.

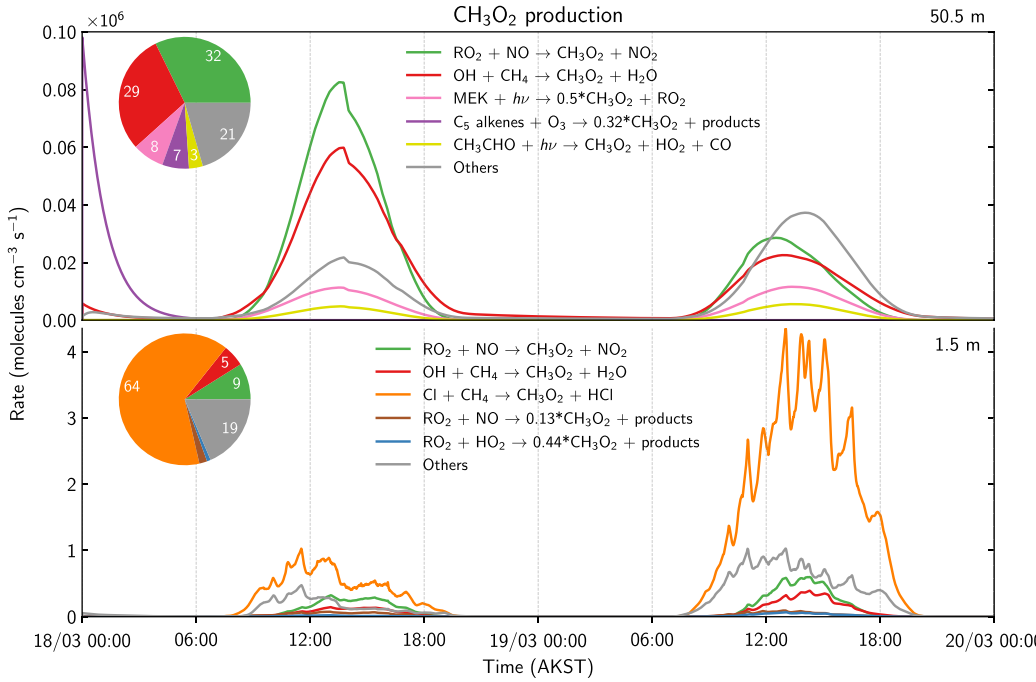


Figure 11. Modeled production reactions of CH_3O_2 at 1.5 and 50.5 m above the snow surface. The five largest contributing reactions are shown for each with the percentage contributions shown as a pie chart.

5.7.2. VOC Chemical Lifetimes

VOCs were measured during the campaign and the impact of Cl and Br atoms on VOC concentrations are discussed in detail in Hornbrook et al. (2016). The influence of chlorine chemistry on VOCs was determined during the campaign by recording the ratio of isobutane to n-butane (iC_4/C_4), as both alkanes react at similar rates with OH, but n-butane reacts approximately 1.5 times faster with Cl. iC_4/C_4 rose over the course of the campaign, indicating increased Cl-atom processing (and Cl_2 production) with increased availability of sunlight as spring progressed. Table 4 shows the simulated OH and Cl atoms concentrations at 1.5 and 50.5 m AGL used to calculate the chemical lifetimes (τ) of several VOCs presented in Table 5. For computational efficiency, some species within the RACM2 mechanism with similar reactivities are lumped together and treated as one species, such as propane and other similar organic compounds (HC3), as well as for pentane (HC5) and octane (HC8). At the surface, Cl atoms are abundant and rapidly oxidize VOCs, typically on the order of several hours, compared to OH which is generally on the order of days. As previously shown, surface OH concentration increases following the addition of halogen emissions, resulting in a reduction of VOC lifetimes by roughly 43% compared to the NOSURF run. This is a significant increase in the reactivity and processing of VOCs via OH due to the presence of halogens. At 50.5 m above the surface, this difference is minimal as levels of halogen radicals are very low, demonstrating the impact of chlorine chemistry close to the ground. We also see a clear gradient in chemical lifetimes with height and would expect longer lived VOCs above the boundary layer to act as a reservoir and replenish surface VOC concentrations by downward transport.

Table 4
OH and Cl Concentrations at 1.5 and 50.5 m, at 12:00 AKST and 48-hr Average in the NOSURF and BASE Runs

	1.5 m		50.5 m	
	12:00 AKST	48-hr average	12:00 AKST	48-hr average
Species	(molecules cm^{-3})		(molecules cm^{-3})	
$[OH]_{NOSURF}$	6.98×10^5	2.37×10^5	3.23×10^5	1.04×10^5
$[OH]_{BASE}$	1.22×10^6	4.57×10^5	3.21×10^5	1.04×10^5
$[Cl]_{BASE}$	7.19×10^5	2.65×10^5	22	7

Indeed, as shown in Hornbrook et al. (2016), the VOCs sampled indicated more important halogen influence on atmospheric chemistry between the early hours of 18 March and 19 March. These VOC observations are likely a mix of local chemistry that is represented within our 1D model and chemistry that occurred while air masses resided over sea ice prior to sampling. Hornbrook et al. (2016) used ethyne levels to show there was a fairly consistent, but moderately low, Br atom influence atmospheric chemistry on 18 March. At the same time, measured acetaldehyde, propanal, and butanal decreased

Table 5
VOC Lifetimes at 1.5 and 50.5 m With Respect to OH and Cl, at 12:00 AKST and 48-hr Average in the NOSURF and BASE Runs

	12:00 AKST			48-hr average		
Species	τ_{OH}^{NOSURF}	τ_{OH}^{BASE}	τ_{Cl}^{BASE}	τ_{OH}^{NOSURF}	τ_{OH}^{BASE}	τ_{Cl}^{BASE}
1.5 m						
HC3	9.7 days	5.5 days	2.8 hr	28.5 days	14.8 days	7.5 hr
HC5[a]	4.4 days	2.5 days	1.6 hr	13.1 days	6.8 days	4.4 hr
HC8[a]	1.8 days	1.0 days	1.1 hr	5.2 days	2.7 days	3.0 hr
Ethane	139 days	79.4 days	7.1 hr	1.1 years	212 days	19.3 hr
Ethene	1.7 days	23.4 hr	2.0 hr	5.0 days	2.6 days	5.3 hr
Acetaldehyde	20.9 hr	12.0 hr	4.8 hr	2.6 days	1.3 days	13.1 hr
Acetone	112 days	64.0 days	11.6 days	329 days	171 days	31.9 days
MEK	15.9 days	9.1 days	9.2 hr	46.9 days	24.3 days	1.0 days
Aldehydes ($\geq C_3$)	15.7 hr	9.0 hr	3.0 hr	1.9 days	1.0 days	8.1 hr
Toluene	2.2 days	1.2 days	6.5 hr	6.4 days	3.3 days	17.8 hr
50.5 m						
HC3	20.8 days	20.9 days	10.3 years	64.6 days	64.6 days	32.4 years
HC5[a]	9.5 days	9.6 days	6.0 years	29.7 days	29.7 days	18.9 years
HC8[a]	3.8 days	3.9 days	4.2 years	11.9 days	11.9 days	13.1 years
Ethane	295 days	297 days	26.6 years	2.5 years	2.5 years	83.5 years
Ethene	3.7 days	3.7 days	7.4 years	11.5 days	11.5 days	23.1 years
Acetaldehyde	1.9 days	1.9 days	18.0 years	5.9 days	5.9 days	56.6 years
Acetone	241 days	243 days	1,042 years	2.1 years	2.1 years	3,275 years
MEK	34.4 days	34.6 days	34.2 years	107 days	107 days	108 years
Aldehydes ($\geq C_3$)	1.4 days	1.4 days	11.1 years	4.4 days	4.4 days	34.9 years
Toluene	4.7 days	4.8 days	24.4 years	14.7 days	14.7 days	76.8 years

Note. HC3, HC5, and HC8 represent lumped hydrocarbon species with similar reactivities and average carbon chains of 3, 5, and 8, respectively. We therefore calculate approximate chemical lifetimes using the rate constants of n-pentane and isopentane (in equal proportions) with Cl for HC5 and n-octane and iso-octane (in equal proportions) with Cl for HC8. Rate constants are obtained from Calvert et al. (2015) at 248 K.

[a]Reactions of HC5 and HC8 with Cl were not included in the chemical mechanism.

by approximately 50%, 75% and 90% respectively (see Figure 14 in Hornbrook et al. (2016)). As well, the butanal observations indicated a gradient between the lowest sampling height, 0.6 m, and the other two sampling heights at 1.5 and 5.4 m, in which the mixing ratio nearest the snow surface reached levels as low as half that at the higher sampling inlets, consistent with Cl atom chemistry near the surface. Overall, our results show that measurements above the Arctic snow surface can be highly influenced by halogen chemistry directly or indirectly via increases in HO_x concentration, resulting in a highly reactive surface layer. Deriving accurate Cl atom concentrations from VOC measurements can therefore be challenging, as surface VOC and Cl atom concentrations are dependent on vertical mixing, surface halogen emissions, and chemistry. In a well-mixed system, downward transport of VOCs can replenish concentrations at the surface, potentially resulting in an underestimation of the derived Cl atom concentration at the ground.

6. Conclusions and Perspectives

In this study, we examined the role of Arctic halogen emissions from snow on boundary layer oxidation processes using an updated version of the PACT-1D model. Snow emissions of Cl_2 and Br_2 were added to the model, including primary production from land-based surface snow and heterogeneous recycling on aerosols and snow.

We compared the model against observations from the 2009 OASIS campaign at Utqiaġvik, Alaska, when high atmospheric Cl_2 levels were observed (18–19 March). The modeled halogen concentrations showed excellent agreement with the observations upon the addition of halogen emissions. The main conclusions of our study can be summarized as follows:

1. Surface Arctic halogen observations are reproduced by the model when including the combined effects of halogen emissions from snow, vertical mixing and atmospheric chemistry. Primary emissions of Cl_2 from snow, parameterized using solar irradiance and measured surface ozone concentration, can describe surface observations of Arctic Cl_2. Modeled Br_2 levels are in good agreement with observations when using a combination of both primary emissions from snow and heterogeneous surface recycling of $BrONO_2$ and HOBr. Sensitivity analyses showed that increased heterogeneous recycling of halogens on aerosols could not explain surface observations and only provided a minor source of reactive halogens in our model simulations (AERO simulation)
2. Boundary layer dynamics, vertical mixing, chemistry and emissions all strongly impact halogen vertical distribution. During the day, Cl_2 is confined to within the lowest 15 m of the atmosphere on both days of the simulation period. Stable conditions during this period resulted in a shallow surface layer, hindering vertical mixing and impacting surface concentrations. In particular, changes in the model vertical mixing and boundary layer dynamics result in a reduction of up to 60 pptv of Cl_2 at 1.5 m during the day (BLD simulation)
3. HO_x radical concentration is increased by up to a factor of 30 with the inclusion of halogen emissions in the model. The increase in OH was primarily driven by elevated HOBr levels and its subsequent photolysis (R6). A significant contributor of HO_2 production is the CH_3O_2 radical formed via the $Cl + CH_4$ reaction (R4). This also caused a decrease in the modeled OH/HO_2 ratio which is attributable to chlorine chemistry
4. Increased HO_x radicals and a high Cl atom concentration near the surface significantly increases chemical reactivity within a shallow layer near the surface. Modeled VOC lifetimes, with respect to OH, are reduced by approximately 43% due to the presence of halogens (BASE run). Cl atoms concentrated near the surface rapidly react with VOCs, but this reactivity becomes much weaker with height and negligible over 15 m above the surface.

We have proposed two model parameterizations for Cl_2 and Br_2 emissions from land-based snow that have been applied to understanding observations during OASIS. Toyota et al. (2011) and recently Marelle et al. (2021) have considered bromine activation, triggered from snow on sea ice, with different efficiency in sunlit compared to dark conditions. In these studies, land-based snow sustains bromine chemistry via conversion of deposited HOBr, $BrONO_2$, and HBr to form Br_2 via reaction of trace quantities of bromide that is assumed to be present in all land-based snow. This is likely too simplified, but works, due to the fact that activated bromine in the atmosphere is lost via deposition and other processes away from the coasts, which also turns off the land-based snow source of Br_2. Here we propose a slightly different approach, which is consistent with our prior modeling study at Summit, Greenland (Thomas et al., 2011) that showed trace amounts of bromide in snow can be activated via photochemistry without enhanced atmospheric bromine already present. This approach is also consistent with the chamber studies presented in Pratt et al. (2013), which showed that land-based snow can release reactive bromine without the need for any other triggers than ozone and sunlight. Land-based snow as a primary source of activated bromine should be tested in 3D regional models using this proposed parameterization, however we note this may not be important regionally compared to the quantities of bromine that are released from snow on sea ice and sea salt aerosols. Physical changes in the snowpack or other properties tied to temperature also influence bromine release from snow on sea ice. For example, Burd et al. (2017) have shown that over the Arctic Ocean atmospheric bromine chemistry is quickly deactivated upon warming to near freezing temperatures and that bromine chemistry is reactivated upon fresh snowfall. The deactivation of bromine release from snow on sea ice upon reaching near freezing temperatures is already included in some models (Marelle et al., 2021; Toyota et al., 2011). At present, less is known on how temperature changes (including related changes in snow physics, impurity locations, etc.) influence bromine release from land-based snow. The inland snow source of reactive bromine is already partially considered in the Toyota et al. (2011) land-based snow treatment which considers all snow to have reactive bromide available for release upon HBr, $BrONO_2$, and HOBr deposition. However, the exact description of how this works is not known and hypotheses should be tested in models and further characterized via observations in the future.

Our modeling work suggests that some description of chlorine emissions from snow is needed to capture the atmospheric chemistry occurring near the surface during Arctic spring. Coastal Arctic surface stations where chlorine has been observed are also the same stations where all long term observations of VOCs, aerosols, and ozone are made. Therefore, understanding and modeling how chlorine contributes to atmospheric chemistry at these locations is essential. We have proposed a model parameterization of chlorine release from land-based snow that depends on available sunlight and ozone. This description needs to be tested during other periods of the year and under different conditions. How this chlorine source depends on other parameters, such as snow chloride content, snow properties, etc., is currently not known due to very limited observations of activated chlorine in the Arctic atmosphere. There is also some evidence that chlorine emissions should be considered from snow on sea ice (e.g., Peterson et al. (2019)). The regional and seasonal sensitivity to potential snow emissions of chlorine needs to be explored with model sensitivity studies using reasonable hypotheses and with dedicated observations in the future.

One of the most important conclusions from our study is that the vertical extent of a highly oxidizing layer with active chlorine chemistry may only extend to 15 m above the snow surface. This is much smaller than the vertical resolution of most regional and global models. The effects of this highly oxidizing layer on new particle formation, aerosol processing, VOC chemistry, and other atmospheric chemistry processes need to be explored and eventually included in models. One possibility is to implement sub-grid scale parameterizations of these processes with regional and global chemical models in the future. The influence of bromine chemistry vertically and with respect to the presence of aerosols and mesoscale weather systems has been relatively well characterized (Blechschmidt et al., 2016; Burd et al., 2017; Liao, Huey, Scheuer, et al., 2012; Oltmans et al., 2012; Peterson et al., 2017; Simpson et al., 2017). However, less is known from observations regarding whether there is active chlorine chemistry above the surface. More observations are needed to quantify both bromine and chlorine chemistry above the surface in order to understand how to best include these effects within models.

Data Availability Statement

The code for the model and input files are all publicly available on Zenodo as Ahmed et al. (2022) https://doi.org/10.5281/zenodo.6045999. The model outputs for the BASE run can also be found on Zenodo at https://doi.org/10.5281/zenodo.5654628. The data for this campaign are publicly available through the NSF Arctic Data Center at https://arcticdata.io/.

Acknowledgments
This work was supported by the Ecole Doctorale Sciences de la Terre, de l'Environnement et des Planètes (ED105) of Université Grenoble Alpes. We also acknowledge support by the CNRS INSU LEFE-CHAT program under the grant Brom-Arc. Shaddy Ahmed and Jennie L. Thomas acknowledge funding from the European Union's Horizon 2020 research and innovation programme under grant agreement No. 101003826 via project CRiceS (Climate Relevant interactions and feedbacks: the key role of sea ice and Snow in the polar and global climate system). This material is based upon work supported by the National Center for Atmospheric Research, which is a major facility sponsored by the National Science Foundation under Cooperative Agreement No. 1852977. We acknowledge support for Detlev Helmig and Patrick Boylan from the NSF Grant 0902165. We acknowledge the additional support to NCAR under the NSF Grant 0806437. We also acknowledge support under the NSF Grant 0732556. We thank the entire OASIS team involved in the campaign and the collection of data with special thanks to: Jin Liao, Andrew Weinheimer, Jim Smith, Roy Mauldin, James Walega, Petter Weibring and Dirk Richter. We also thank colleagues Aurélien Dommergue, Didier Voisin, Pierre Rampal, Anna Jones and Thorsten Bartels-Rausch for meaningful scientific discussions.

References

Abbatt, J. P. D., Thomas, J. L., Abrahamsson, K., Boxe, C., Granfors, A., Jones, A. E., et al. (2012). Halogen activation via interactions with environmental ice and snow in the polar lower troposphere and other regions. *Atmospheric Chemistry and Physics*, *12*(14), 6237–6271. https://doi.org/10.5194/acp-12-6237-2012

Aguzzi, A., & Rossi, J. M. (1999). The kinetics of the heterogeneous reaction of $BrONO_2$ with solid alkali halides at ambient temperature. A comparison with the interaction of $ClONO_2$ on NaCl and KBr. *Physical Chemistry Chemical Physics*, *1*, 4337–4346. https://doi.org/10.1039/A904611I

Ahmed, S., Thomas, J. L., Tuite, K., & Stutz, J. (2022). *PACT-1D model (v1.1) including polar chlorine and bromine emission mechanisms*. Zenodo. https://doi.org/10.5281/zenodo.6045999

Ammann, M., Cox, R. A., Crowley, J. N., Jenkin, M. E., Mellouki, A., Rossi, M. J., et al. (2013). Evaluated kinetic and photochemical data for atmospheric chemistry: Volume VI—Heterogeneous reactions with liquid substrates. *Atmospheric Chemistry and Physics*, *13*(16), 8045–8228. https://doi.org/10.5194/acp-13-8045-2013

Anderson, P. S., & Neff, W. D. (2008). Boundary layer physics over snow and ice. *Atmospheric Chemistry and Physics*, *8*(13), 3563–3582. https://doi.org/10.5194/acp-8-3563-2008

Apel, E. C. (2009). *VOC measurements during OASIS Barrow field intensive Spring 2009*. Arctic Data Center. https://doi.org/10.5065/D6DB7ZXF

Atkinson, R., Baulch, D. L., Cox, R. A., Crowley, J. N., Hampson, R. F., Hynes, R. G., et al. (2006). Evaluated kinetic and photochemical data for atmospheric chemistry: Volume II—Gas phase reactions of organic species. *Atmospheric Chemistry and Physics*, *6*(11), 3625–4055. https://doi.org/10.5194/acp-6-3625-2006

Barret, M., Domine, F., Houdier, S., Gallet, J.-C., Weibring, P., Walega, J., et al. (2011). Formaldehyde in the Alaskan Arctic snowpack: Partitioning and physical processes involved in air-snow exchanges. *Journal of Geophysical Research: Atmospheres*, *116*(D14). https://doi.org/10.1029/2011JD016038

Barrie, L. A., Bottenheim, J. W., Schnell, R. C., Crutzen, P. J., & Rasmussen, R. A. (1988). Ozone destruction and photochemical reactions at polar sunrise in the lower Arctic atmosphere. *Nature*, *334*(6178), 138–141. https://doi.org/10.1038/334138a0

Bartels-Rausch, T., Jacobi, H.-W., Kahan, T. F., Thomas, J. L., Thomson, E. S., Abbatt, J. P. D., et al. (2014). A review of air–ice chemical and physical interactions (AICI): Liquids, quasi-liquids, and solids in snow. *Atmospheric Chemistry and Physics*, *14*(3), 1587–1633. https://doi.org/10.5194/acp-14-1587-2014

Blechschmidt, A.-M., Richter, A., Burrows, J. P., Kaleschke, L., Strong, K., Theys, N., et al. (2016). An exemplary case of a bromine explosion event linked to cyclone development in the Arctic. *Atmospheric Chemistry and Physics*, *16*(3), 1773–1788. https://doi.org/10.5194/acp-16-1773-2016

Boylan, P., Helmig, D., Staebler, R., Turnipseed, A., Fairall, C., & Neff, W. (2014). Boundary layer dynamics during the Ocean-Atmosphere-Sea-Ice-Snow (OASIS) 2009 experiment at Barrow, AK. *Journal of Geophysical Research: Atmospheres*, *119*(5), 2261–2278. https://doi.org/10.1002/2013JD020299

Brioude, J., Arnold, D., Stohl, A., Cassiani, M., Morton, D., Seibert, P., et al. (2013). The Lagrangian particle dispersion model FLEXPART-WRF version 3.1. *Geoscientific Model Development*, *6*(6), 1889–1904. https://doi.org/10.5194/gmd-6-1889-2013

Buchholz, R. R., Emmons, L. K., Tilmes, S., & The CESM2 Development Team. (2019). CESM2.1/CAM-chem instantaneous output for boundary conditions. *UCAR/NCAR—Atmospheric chemistry observations and modeling Laboratory. Subset used Lat: 50 to 90, Lon: 120 to 250, 18 March 2009–18 March 2009*. https://doi.org/10.5065/NMP7-EP60

Burd, J. A., Peterson, P. K., Nghiem, S. V., Perovich, D. K., & Simpson, W. R. (2017). Snowmelt onset hinders bromine monoxide heterogeneous recycling in the Arctic. *Journal of Geophysical Research: Atmospheres*, *122*(15), 8297–8309. https://doi.org/10.1002/2017JD026906

Burkholder, J. B., Sander, S. P., Abbatt, J., Barker, J. R., Cappa, C., Crounse, J. D., & Wine, P. H. (2019). *Chemical kinetics and photochemical data for use in Atmospheric Studies, Evaluation No. 19*. JPL Publication 19-5, Jet Propulsion Laboratory. Retrieved from http://jpldataeval.jpl.nasa.gov/

Calvert, J. G., Orlando, J. J., Stockwell, W. R., & Wallington, T. J. (2015). *The mechanisms of reactions influencing atmospheric ozone*. Oxford University Press.

Cantrell, C. A. (2009). *HO_2 and RO_2 measurements during OASIS Barrow field intensive Spring 2009*. Arctic Data Center. https://doi.org/10.5065/D6GH9G2J

Cao, L., Platt, U., & Gutheil, E. (2016). Role of the boundary layer in the occurrence and termination of the tropospheric ozone depletion events in polar spring. *Atmospheric Environment*, *132*, 98–110. https://doi.org/10.1016/j.atmosenv.2016.02.034

Custard, K. D., Thompson, C. R., Pratt, K. A., Shepson, P. B., Liao, J., Huey, L. G., et al. (2015). The NO_x dependence of bromine chemistry in the Arctic atmospheric boundary layer. *Atmospheric Chemistry and Physics*, *15*(18), 10799–10809. https://doi.org/10.5194/acp-15-10799-2015

Custard, K. D., Pratt, K. A., Wang, S., & Shepson, P. B. (2016). Constraints on Arctic atmospheric chlorine production through measurements and simulations of Cl_2 and ClO. *Environmental Science and Technology*, *50*(22), 12394–12400. https://doi.org/10.1021/acs.est.6b03909

Custard, K. D., Raso, A. R. W., Shepson, P. B., Staebler, R. M., & Pratt, K. A. (2017). Production and release of molecular bromine and chlorine from the Arctic coastal snowpack. *ACS Earth and Space Chemistry*, *1*(3), 142–151. https://doi.org/10.1021/acsearthspacechem.7b00014

Deiber, G., George, C., Le Calvé, S., Schweitzer, F., & Mirabel, P. (2004). Uptake study of $ClONO_2$ and $BrONO_2$ by Halide containing droplets. *Atmospheric Chemistry and Physics*, *4*(5), 1291–1299. https://doi.org/10.5194/acp-4-1291-2004

Domine, F., Albert, M., Huthwelker, T., Jacobi, H.-W., Kokhanovsky, A. A., Lehning, M., et al. (2008). Snow physics as relevant to snow photochemistry. *Atmospheric Chemistry and Physics*, *8*(2), 171–208. https://doi.org/10.5194/acp-8-171-2008

Domine, F., Bock, J., Voisin, D., & Donaldson, D. J. (2013). Can we model snow photochemistry? Problems with the current approaches. *The Journal of Physical Chemistry A*, *117*(23), 4733–4749. https://doi.org/10.1021/jp3123314

Durre, I., Vose, R. S., & Wuertz, D. B. (2006). Overview of the integrated global radiosonde archive. *Journal of Climate*, *19*(1), 53–68. https://doi.org/10.1175/JCLI3594.1

Emmons, L. K., Schwantes, R. H., Orlando, J. J., Tyndall, G., Kinnison, D., Lamarque, J.-F., et al. (2020). The chemistry mechanism in the community Earth System Model version 2 (CESM2). *Journal of Advances in Modeling Earth Systems*, *12*(4), e2019MS001882. https://doi.org/10.1029/2019MS001882

Falk, S., & Sinnhuber, B.-M. (2018). Polar boundary layer bromine explosion and ozone depletion events in the chemistry–climate model EMAC v2.52: Implementation and evaluation of AirSnow algorithm. *Geoscientific Model Development*, *11*(3), 1115–1131. https://doi.org/10.5194/gmd-11-1115-2018

Fernandez, R. P., Carmona-Balea, A., Cuevas, C. A., Barrera, J. A., Kinnison, D. E., Lamarque, J.-F., et al. (2019). Modeling the sources and chemistry of polar tropospheric halogens (Cl, Br, and I) using the CAM-chem global chemistry-climate Model. *Journal of Advances in Modeling Earth Systems*, *11*(7), 2259–2289. https://doi.org/10.1029/2019MS001655

Finlayson-Pitts, B. J., Ezell, M. J., & Pitts, J. N. (1989). Formation of chemically active chlorine compounds by reactions of atmospheric NaCl particles with gaseous N_2O_5 and $ClONO_2$. *Nature*, *337*(6204), 241–244. https://doi.org/10.1038/337241a0

Frey, M. M., Roscoe, H. K., Kukui, A., Savarino, J., France, J. L., King, M. D., et al. (2015). Atmospheric nitrogen oxides (NO and NO_2) at Dome C, East Antarctica, during the OPALE campaign. *Atmospheric Chemistry and Physics*, *15*(14), 7859–7875. https://doi.org/10.5194/acp-15-7859-2015

Fried, A. (2009). *Formaldehyde measurements during OASIS Barrow field intensive Spring 2009*. Arctic Data Center. https://doi.org/10.5065/D63B5X7H

Goliff, W. S., Stockwell, W. R., & Lawson, C. V. (2013). The regional atmospheric chemistry mechanism, version 2. *Atmospheric Environment*, *68*, 174–185. https://doi.org/10.1016/j.atmosenv.2012.11.038

Grannas, A. M., Jones, A. E., Dibb, J., Ammann, M., Anastasio, C., Beine, H. J., et al. (2007). An overview of snow photochemistry: Evidence, mechanisms and impacts. *Atmospheric Chemistry and Physics*, *7*(16), 4329–4373. https://doi.org/10.5194/acp-7-4329-2007

Guenther, A. B. (2009). *Meteorology measurements during OASIS Barrow field intensive Spring 2009*. Arctic Data Center. https://doi.org/10.5065/D62J6902

Hall, S. R. (2009). *Actinic flux measurements during OASIS barrow field intensive Spring 2009*. Arctic Data Center. https://doi.org/10.5065/D6GB2260

Helmig, D., Boylan, P., Johnson, B., Oltmans, S., Fairall, C., Staebler, R., et al. (2012). Ozone dynamics and snow-atmosphere exchanges during ozone depletion events at Barrow, Alaska. *Journal of Geophysical Research*, *117*, D20303. https://doi.org/10.1029/2012JD017531

Herrmann, M., Cao, L., Sihler, H., Platt, U., & Gutheil, E. (2019). On the contribution of chemical oscillations to ozone depletion events in the polar spring. *Atmospheric Chemistry and Physics*, *19*(15), 10161–10190. https://doi.org/10.5194/acp-19-10161-2019

Herrmann, M., Sihler, H., Frieß, U., Wagner, T., Platt, U., & Gutheil, E. (2021). Time-dependent 3D simulations of tropospheric ozone depletion events in the Arctic spring using the Weather Research and Forecasting model coupled with Chemistry (WRF-Chem). *Atmospheric Chemistry and Physics*, *21*(10), 7611–7638. https://doi.org/10.5194/acp-21-7611-2021

Honrath, R. E., Peterson, M. C., Guo, S., Dibb, J. E., Shepson, P. B., & Campbell, B. (1999). Evidence of NO_x production within or upon ice particles in the Greenland snowpack. *Geophysical Research Letters*, *26*(6), 695–698. https://doi.org/10.1029/1999GL900077

Honrath, R. E., Lu, Y., Peterson, M. C., Dibb, J. E., Arsenault, M. A., Cullen, N. J., & Steffen, K. (2002). Vertical fluxes of NO_x, HONO, and HNO_3 above the snowpack at Summit, Greenland. *Atmospheric Environment*, *36*(15), 2629–2640. https://doi.org/10.1016/S1352-2310(02)00132-2

Hornbrook, R. S., Crawford, J. H., Edwards, G. D., Goyea, O., Mauldin, R. L., III, Olson, J. S., & Cantrell, C. A. (2011). Measurements of tropospheric HO_2 and RO_2 by oxygen dilution modulation and chemical ionization mass spectrometry. *Atmospheric Measurement Techniques*, *4*(4), 735–756. https://doi.org/10.5194/amt-4-735-2011

Hornbrook, R. S., Hills, A. J., Riemer, D. D., Abdelhamid, A., Flocke, F. M., Hall, S. R., et al. (2016). Arctic springtime observations of volatile organic compounds during the OASIS-2009 campaign. *Journal of Geophysical Research: Atmospheres*, *121*(16), 9789–9813. https://doi.org/10.1002/2015JD024360

Hu, J. H., Shi, Q., Davidovits, P., Worsnop, D. R., Zahniser, M. S., & Kolb, C. E. (1995). Reactive uptake of $Cl_{2(g)}$ and $Br_{2(g)}$ by aqueous surfaces as a function of Br^- and I^- ion concentration: The effect of chemical reaction at the interface. *The Journal of Physical Chemistry*, *99*(21), 8768–8776. https://doi.org/10.1021/j100021a050

IUPAC. (2009). *IUPAC task group on atmospheric chemical kinetic data Evaluation*. Retrieved from https://iupac-aeris.ipsl.fr/

Kahl, J. D. (1990). Characteristics of the low-level temperature inversion along the Alaskan Arctic coast. *International Journal of Climatology*, *10*(5), 537–548. https://doi.org/10.1002/joc.3370100509

Knipping, E. M., Lakin, M. J., Foster, K. L., Jungwirth, P., Tobias, D. J., Gerber, R. B., et al. (2000). Experiments and simulations of ion-enhanced interfacial chemistry on aqueous NaCl aerosols. *Science*, *288*(5464), 301–306. https://doi.org/10.1126/science.288.5464.301

Laskin, A., Wang, H., Robertson, W. H., Cowin, J. P., Ezell, M. J., & Finlayson-Pitts, B. J. (2006). A new approach to determining gas-particle reaction probabilities and application to the heterogeneous reaction of deliquesced sodium chloride particles with gas-phase hydroxyl radicals. *The Journal of Physical Chemistry A*, *110*(36), 10619–10627. https://doi.org/10.1021/jp063263+

Lehrer, E., Hönninger, G., & Platt, U. (2004). A one dimensional model study of the mechanism of halogen liberation and vertical transport in the polar troposphere. *Atmospheric Chemistry and Physics*, *4*, 2427–2440. https://doi.org/10.5194/acp-4-2427-2004

Liao, J., Huey, L. G., Liu, Z., Tanner, D. J., Cantrell, C. A., Orlando, J. J., et al. (2014). High levels of molecular chlorine in the Arctic atmosphere. *Nature Geoscience*, *7*(2), 91–94. https://doi.org/10.1038/ngeo2046

Liao, J., Huey, L. G., Scheuer, E., Dibb, J. E., Stickel, R. E., Tanner, D. J., et al. (2012). Characterization of soluble bromide measurements and a case study of BrO observations during ARCTAS. *Atmospheric Chemistry and Physics*, *12*(3), 1327–1338. https://doi.org/10.5194/acp-12-1327-2012

Liao, J., Huey, L. G., Tanner, D. J., Flocke, F. M., Orlando, J. J., Neuman, J. A., et al. (2012). Observations of inorganic bromine (HOBr, BrO, and Br_2) speciation at Barrow, Alaska, in spring 2009. *Journal of Geophysical Research*, *117*, D00R16. https://doi.org/10.1029/2011JD016641

Liao, J., Sihler, H., Huey, L. G., Neuman, J. A., Tanner, D. J., Friess, U., et al. (2011). A comparison of Arctic BrO measurements by chemical ionization mass spectrometry and long path-differential optical absorption spectroscopy. *Journal of Geophysical Research*, *116*, D00R02. https://doi.org/10.1029/2010JD014788

Liu, X., Qu, H., Huey, L. G., Wang, Y., Sjostedt, S., Zeng, L., et al. (2017). High levels of daytime molecular chlorine and nitryl chloride at a rural site on the North China plain. *Environmental Science & Technology*, *51*(17), 9588–9595. https://doi.org/10.1021/acs.est.7b03039

Madronich, S., & Flocke, S. (1999). The role of solar radiation in atmospheric chemistry. In *The handbook of environmental photochemistry* (pp. 1–26). Springer. https://doi.org/10.1007/978-3-540-69044-3_1

Marelle, L., Raut, J.-C., Law, K. S., Berg, L. K., Fast, J. D., Easter, R. C., et al. (2017). Improvements to the WRF-Chem 3.5.1 model for quasi-hemispheric simulations of aerosols and ozone in the Arctic. *Geoscientific Model Development*, *10*(10), 3661–3677. https://doi.org/10.5194/gmd-10-3661-2017

Marelle, L., Thomas, J. L., Ahmed, S., Tuite, K., Stutz, J., Dommergue, A., et al. (2021). Implementation and impacts of surface and blowing snow sources of Arctic bromine activation within WRF-Chem 4.1.1. *Journal of Advances in Modeling Earth Systems*, *13*, e2020MS002391. https://doi.org/10.1029/2020MS002391

Mauldin, R. L., III, Frost, G. J., Chen, G., Tanner, D. J., Prevot, A. S. H., Davis, D. D., & Eisele, F. L. (1998). OH measurements during the first aerosol characterization experiment (ACE 1): Observations and model comparisons. *Journal of Geophysical Research*, *103*(D13), 16713–16729. https://doi.org/10.1029/98JD00882

McNamara, S. M., Raso, A. R. W., Wang, S., Thanekar, S., Boone, E. J., Kolesar, K. R., et al. (2019). Springtime nitrogen oxide-influenced chlorine chemistry in the coastal Arctic. *Environmental Science & Technology*, *53*(14), 8057–8067. https://doi.org/10.1021/acs.est.9b01797

McNamara, S. M., Garner, N. M., Wang, S., Raso, A. R. W., Thanekar, S., Barget, A. J., et al. (2020). Bromine chloride in the coastal Arctic: Diel patterns and production mechanisms. *ACS Earth and Space Chemistry*, *4*(4), 620–630. https://doi.org/10.1021/acsearthspacechem.0c00021

McNamara, S. M., Chen, Q., Edebeli, J., Kulju, K. D., Mumpfield, J., Fuentes, J. D., et al. (2021). Observation of N_2O_5 deposition and $ClNO_2$ production on the saline snowpack. *ACS Earth and Space Chemistry*, *5*(5), 1020–1031. https://doi.org/10.1021/acsearthspacechem.0c00317

McNeill, V. F., Grannas, A. M., Abbatt, J. P. D., Ammann, M., Ariya, P., Bartels-Rausch, T., et al. (2012). Organics in environmental ices: Sources, chemistry, and impacts. *Atmospheric Chemistry and Physics*, *12*(20), 9653–9678. https://doi.org/10.5194/acp-12-9653-2012

Moore, C. W., Obrist, D., Steffen, A., Staebler, R. M., Douglas, T. A., Richter, A., & Nghiem, S. V. (2014). Convective forcing of mercury and ozone in the Arctic boundary layer induced by leads in sea ice. *Nature*, *506*(7486), 81–84. https://doi.org/10.1038/nature12924

Neff, W., Helmig, D., Grachev, A., & Davis, D. (2008). A study of boundary layer behavior associated with high NO concentrations at the South Pole using a minisodar, tethered balloon, and sonic anemometer. *Atmospheric Environment*, *42*(12), 2762–2779. https://doi.org/10.1016/j.atmosenv.2007.01.033

Oltmans, S. J., Johnson, B. J., & Harris, J. M. (2012). Springtime boundary layer ozone depletion at Barrow, Alaska: Meteorological influence, year-to-year variation, and long-term change. *Journal of Geophysical Research*, *117*, D00R18. https://doi.org/10.1029/2011JD016889

Parrish, D. D., Holloway, J. S., & Fehsenfeld, F. C. (1994). Routine, continuous measurement of carbon monoxide with parts per billion precision. *Environmental Science & Technology*, *28*(9), 1615–1618. https://doi.org/10.1021/es00058a013

Peterson, P. K., Simpson, W. R., Pratt, K. A., Shepson, P. B., Frieß, U., Zielcke, J., et al. (2015). Dependence of the vertical distribution of bromine monoxide in the lower troposphere on meteorological factors such as wind speed and stability. *Atmospheric Chemistry and Physics*, *15*(4), 2119–2137. https://doi.org/10.5194/acp-15-2119-2015

Peterson, P. K., Pöhler, D., Sihler, H., Zielcke, J., General, S., Frieß, U., et al. (2017). Observations of bromine monoxide transport in the Arctic sustained on aerosol particles. *Atmospheric Chemistry and Physics*, *17*(12), 7567–7579. https://doi.org/10.5194/acp-17-7567-2017

Peterson, P. K., Hartwig, M., May, N. W., Schwartz, E., Rigor, I., Ermold, W., et al. (2019). Snowpack measurements suggest role for multi-year sea ice regions in Arctic atmospheric bromine and chlorine chemistry. *Elementa: Science of the Anthropocene*, *7*. https://doi.org/10.1525/elementa.352

Piot, M., & von Glasow, R. (2008). The potential importance of frost flowers, recycling on snow, and open leads for ozone depletion events. *Atmospheric Chemistry and Physics*, *8*(9), 2437–2467. https://doi.org/10.5194/acp-8-2437-2008

Piot, M., & von Glasow, R. (2009). Modelling the multiphase near-surface chemistry related to ozone depletions in polar spring. *Journal of Atmospheric Chemistry*, *64*(2), 77–105. https://doi.org/10.1007/s10874-010-9170-1

Platt, U., & Hönninger, G. (2003). The role of halogen species in the troposphere. *Chemosphere*, *52*(2), 325–338. https://doi.org/10.1016/S0045-6535(03)00216-9

Pollard, R. T., Rhines, P. B., & Thompson, R. O. R. Y. (1973). The deepening of the wind-Mixed layer. *Geophysical Fluid Dynamics*, *4*(4), 381–404. https://doi.org/10.1080/03091927208236105

Pratt, K. A., Custard, K. D., Shepson, P. B., Douglas, T. A., Pöhler, D., General, S., et al. (2013). Photochemical production of molecular bromine in Arctic surface snowpacks. *Nature Geoscience*, *6*(5), 351–356. https://doi.org/10.1038/ngeo1779

Pratte, P., & Rossi, M. J. (2006). The heterogeneous kinetics of HOBr and HOCl on acidified sea salt and model aerosol at 40–90% relative humidity and ambient temperature. *Physical Chemistry Chemical Physics*, *8*, 3988–4001. https://doi.org/10.1039/B604321F

Rudolph, J., Ru Fu, B., Thompson, A., Anlauf, K., & Bottenheim, J. (1999). Halogen atom concentrations in the Arctic Troposphere derived from hydrocarbon measurements: Impact on the budget of formaldehyde. *Geophysical Research Letters*, *26*(19), 2941–2944. https://doi.org/10.1029/1999GL010869

Sandu, A., & Sander, R. (2006). Technical note: Simulating chemical systems in Fortran90 and Matlab with the kinetic PreProcessor KPP-2.1. *Atmospheric Chemistry and Physics*, *6*(1), 187–195. https://doi.org/10.5194/acp-6-187-2006

Seisel, S., Flückiger, B., & Rossi, M. J. (1998). The heterogeneous reaction of N_2O_5 with HBr on Ice comparison with N_2O_5+HCl. *Berichte der Bunsengesellschaft für physikalische Chemie*, *102*(6), 811–820. https://doi.org/10.1002/bbpc.19981020604

Shetter, R. E., & Müller, M. (1999). Photolysis frequency measurements using actinic flux spectroradiometry during the PEM-Tropics mission: Instrumentation description and some results. *Journal of Geophysical Research*, *104*(D5), 5647–5661. https://doi.org/10.1029/98JD01381

Simpson, W. R., Brown, S. S., Saiz-Lopez, A., Thornton, J. A., & von Glasow, R. (2015). Tropospheric halogen chemistry: Sources, cycling, and impacts. *Chemical Reviews*, *115*(10), 4035–4062. https://doi.org/10.1021/cr5006638

Simpson, W. R., Peterson, P. K., Frieß, U., Sihler, H., Lampel, J., Platt, U., et al. (2017). Horizontal and vertical structure of reactive bromine events probed by bromine monoxide MAX-DOAS. *Atmospheric Chemistry and Physics*, *17*(15), 9291–9309. https://doi.org/10.5194/acp-17-9291-2017

Simpson, W. R., von Glasow, R., Riedel, K., Anderson, P., Ariya, P., Bottenheim, J., et al. (2007). Halogens and their role in polar boundary-layer ozone depletion. *Atmospheric Chemistry and Physics*, *7*(16), 4375–4418. https://doi.org/10.5194/acp-7-4375-2007

Skamarock, W. C., Klemp, J. B., Dudhia, J., Gill, D. O., Liu, Z., Berner, J., et al. (2019). *A description of the advanced Research WRF version 4. (Tech. Rep.)* (p. 145). Note NCAR/TN-556+STR. https://doi.org/10.5065/1dfh-6p97

Smith, J., Sjostedt, S., Abbatt, J., & Wiedensohler, A. (2009). *Aerosol measurements during OASIS Barrow field intensive Spring 2009*. Arctic Data Center. https://doi.org/10.5065/D6P8491K

Steffen, A., Bottenheim, J., Cole, A., Douglas, T. A., Ebinghaus, R., Friess, U., et al. (2013). Atmospheric mercury over sea ice during the OASIS-2009 campaign. *Atmospheric Chemistry and Physics*, *13*(14), 7007–7021. https://doi.org/10.5194/acp-13-7007-2013

Steffen, A., Douglas, T., Amyot, M., Ariya, P., Aspmo, K., Berg, T., et al. (2008). A synthesis of atmospheric mercury depletion event chemistry in the atmosphere and snow. *Atmospheric Chemistry and Physics*, *8*(6), 1445–1482. https://doi.org/10.5194/acp-8-1445-2008

Tanner, D. J., Jefferson, A., & Eisele, F. L. (1997). Selected ion chemical ionization mass spectrometric measurement of OH. *Journal of Geophysical Research*, *102*(D5), 6415–6425. https://doi.org/10.1029/96JD03919

Thomas, J. L., Dibb, J. E., Huey, L. G., Liao, J., Tanner, D., Lefer, B., et al. (2012). Modeling chemistry in and above snow at Summit, Greenland—Part 2: Impact of snowpack chemistry on the oxidation capacity of the boundary layer. *Atmospheric Chemistry and Physics*, *12*(14), 6537–6554. https://doi.org/10.5194/acp-12-6537-2012

Thomas, J. L., Stutz, J., Lefer, B., Huey, L. G., Toyota, K., Dibb, J. E., & von Glasow, R. (2011). Modeling chemistry in and above snow at Summit, Greenland—Part 1: Model description and results. *Atmospheric Chemistry and Physics*, *11*(10), 4899–4914. https://doi.org/10.5194/acp-11-4899-2011

Thompson, C. R., Shepson, P. B., Liao, J., Huey, L. G., Apel, E. C., Cantrell, C. A., et al. (2015). Interactions of bromine, chlorine, and iodine photochemistry during ozone depletions in Barrow, Alaska. *Atmospheric Chemistry and Physics*, *15*(16), 9651–9679. https://doi.org/10.5194/acp-15-9651-2015

Toyota, K., McConnell, J. C., Lupu, A., Neary, L., McLinden, C. A., Richter, A., et al. (2011). Analysis of reactive bromine production and ozone depletion in the Arctic boundary layer using 3-D simulations with GEM-AQ: Inference from synoptic-scale patterns. *Atmospheric Chemistry and Physics*, *11*(8), 3949–3979. https://doi.org/10.5194/acp-11-3949-2011

Toyota, K., McConnell, J. C., Staebler, R. M., & Dastoor, A. P. (2014). Air–snowpack exchange of bromine, ozone and mercury in the springtime Arctic simulated by the 1-D model PHANTAS—Part 1: In-snow bromine activation and its impact on ozone. *Atmospheric Chemistry and Physics*, *14*(8), 4101–4133. https://doi.org/10.5194/acp-14-4101-2014

Tuite, K., Thomas, J. L., Veres, P. R., Roberts, J. M., Stevens, P. S., Griffith, S. M., et al. (2021). Quantifying nitrous acid formation mechanisms using measured vertical profiles during the CalNex 2010 campaign and 1D column modeling. *Journal of Geophysical Research: Atmospheres*, *126*, e2021JD034689. https://doi.org/10.1029/2021JD034689

Villena, G., Wiesen, P., Cantrell, C. A., Flocke, F., Fried, A., Hall, S. R., et al. (2011). Nitrous acid (HONO) during polar spring in Barrow, Alaska: A net source of OH radicals? *Journal of Geophysical Research*, *116*, D00R07. https://doi.org/10.1029/2011JD016643

Wang, S., McNamara, S. M., Kolesar, K. R., May, N. W., Fuentes, J. D., Cook, R. D., et al. (2020). Urban snowpack $ClNO_2$ production and fate: A one-dimensional modeling Study. *ACS Earth and Space Chemistry*, *4*(7), 1140–1148. https://doi.org/10.1021/acsearthspacechem.0c00116

Wang, S., McNamara, S. M., Moore, C. W., Obrist, D., Steffen, A., Shepson, P. B., et al. (2019). Direct detection of atmospheric atomic bromine leading to mercury and ozone depletion. *Proceedings of the National Academy of Sciences*, *116*(29), 14479–14484. https://doi.org/10.1073/pnas.1900613116

Wang, S., & Pratt, K. A. (2017). Molecular halogens above the arctic snowpack: Emissions, diurnal variations, and recycling mechanisms. *Journal of Geophysical Research: Atmospheres*, *122*(21), 11991–12007. https://doi.org/10.1002/2017JD027175

Weibring, P., Richter, D., Walega, J. G., & Fried, A. (2007). First demonstration of a high performance difference frequency spectrometer on airborne platforms. *Optics Express*, *15*(21), 13476–13495. https://doi.org/10.1364/OE.15.013476

Weibring, P., Richter, D., Walega, J. G., Rippe, L., & Fried, A. (2010). Difference frequency generation spectrometer for simultaneous multispecies detection. *Optics Express*, *18*(26), 27670–27681. https://doi.org/10.1364/OE.18.027670

Weinheimer, A. J. (2009). *Ozone, NOx, and NOy measurements during OASIS Barrow field intensive Spring 2009*. Arctic Data Center. https://doi.org/10.5065/D6RJ4GK6

Weinheimer, A. J., Montzka, D. D., Campos, T. L., Walega, J. G., Ridley, B. A., Donnelly, S. G., et al. (1998). Comparison between DC-8 and ER-2 species measurements in the tropical middle troposphere: NO, NO_y, O_3, CO_2, CH_4, and N_2O. *Journal of Geophysical Research*, *103*(D17), 22087–22096. https://doi.org/10.1029/98JD01421

Willmes, S., & Heinemann, G. (2015). Daily pan-Arctic sea-ice lead maps for 2003–2015, with links to maps in NetCDF format. *PANGAEA*. https://doi.org/10.1594/PANGAEA.854411

Willmes, S., & Heinemann, G. (2016). Sea-Ice wintertime lead frequencies and regional characteristics in the Arctic, 2003–2015. *Remote Sensing*, *8*(1). https://doi.org/10.3390/rs8010004

Woo, K. S., Chen, D. R., Pui, D. Y. H., & McMurry, P. H. (2001). Measurement of Atlanta aerosol size distributions: Observations of ultrafine particle events. *Aerosol Science and Technology*, *34*(1), 75–87. https://doi.org/10.1080/02786820120056

Zilitinkevich, S., & Baklanov, A. (2002). Calculation of the height of the stable boundary layer in practical applications. *Boundary-Layer Meteorology*, *105*(3), 389–409. https://doi.org/10.1023/A:1020376832738

Zilitinkevich, S., Baklanov, A., Rost, J., Smedman, A.-s., Lykosov, V., & Calanca, P. (2002). Diagnostic and prognostic equations for the depth of the stably stratified Ekman boundary layer. *Quarterly Journal of the Royal Meteorological Society*, *128*(579), 25–46. https://doi.org/10.1256/00359000260498770